Chapter 2

Aerodynamic Model

2.1 The Navier-Stokes Equations

The Navier-Stokes equations for a fluid with constant density ρ and kinematic viscosity ν and subject to body forces per unit mass $\mathbf{F}$ are expressible in terms of the velocity $\mathbf{V} = \mathbf{V}(\mathbf{R}, t)$ and the pressure $p = p(\mathbf{R}, t)$ where $\mathbf{R}$ is the position in space and t is the time as

$$\frac{\partial \mathbf{V}}{\partial t} + (\mathbf{V} \cdot \boldsymbol{\nabla})\ \mathbf{V} = -\frac{1}{\rho}\boldsymbol{\nabla} p + \nu \boldsymbol{\nabla}^2 \mathbf{V} + \mathbf{F} \tag{2.1}$$

Together with the continuity equation for incompressible flow

$$\boldsymbol{\nabla} \cdot \mathbf{V} = 0 \tag{2.2}$$

they form a set of four scalar differential equations sufficient for the determination of $\mathbf{V}(\mathbf{R}, t)$ and $p(\mathbf{R}, t)$, provided that adequate initial and boundary conditions are known. The boundary conditions occurring most frequently are the "no-slip" condition at the surface of the solid over which the fluid passes [159]. For problems involving an infinite domain, $\mathbf{V}(\mathbf{R}, t)$ and $p(\mathbf{R}, t)$ at infinity must also be specified.

It is convenient to introduce the vorticity field of the flow $\boldsymbol{\Omega}(\mathbf{R}, t)$ defined by

$$\boldsymbol{\Omega} = \boldsymbol{\nabla} \times \mathbf{V} \tag{2.3}$$

$$= 2\,\boldsymbol{\omega} \tag{2.4}$$

where $\boldsymbol{\omega} = \boldsymbol{\omega}(\mathbf{R}, t)$ is the angular velocity field of the flow. In homogeneous fluids, vorticity is produced only where there are shear stresses such as at the boundaries of the fluid region or where two streams with different velocities merge. Vorticity can also be generated in the interior of inhomogeneous fluids or at a free surface when gravity is acting. However, in this thesis, we restrict our discussion to an homogeneous incompressible fluid.

The vorticity transport equation for a fluid of uniform density ρ and kinematic viscosity ν subjected to only irrotational body forces (i.e., $\boldsymbol{\nabla} \times \mathbf{F} = \mathbf{0}$) is obtained by taking the curl of both sides of (2.1) in the form

$$\frac{\partial \boldsymbol{\Omega}}{\partial t} = \boldsymbol{\nabla} \times (\mathbf{V} \times \boldsymbol{\Omega}) + \nu \boldsymbol{\nabla}^2 \boldsymbol{\Omega} \tag{2.5}$$

in which use is made of the relations (2.2) and (2.3). Making use of the following vector/tensor identities

$$\mathbf{F} \times (\mathbf{G} \times \mathbf{H}) = (\mathbf{F} \cdot \mathbf{H})\,\mathbf{G} - (\mathbf{F} \cdot \mathbf{G})\,\mathbf{H}$$

$$\begin{aligned} \mathbf{G} \cdot \boldsymbol{\nabla}\mathbf{F} &= \frac{1}{2}[\boldsymbol{\nabla}(\mathbf{G} \cdot \mathbf{F}) - \mathbf{G} \times (\boldsymbol{\nabla} \times \mathbf{F}) - \mathbf{F} \times (\boldsymbol{\nabla} \times \mathbf{G}) \\ &- \boldsymbol{\nabla} \times (\mathbf{G} \times \mathbf{F}) + \mathbf{G}(\boldsymbol{\nabla} \cdot \mathbf{F}) - \mathbf{F}(\boldsymbol{\nabla} \cdot \mathbf{G})] \end{aligned}$$

we can rewrite Equation (2.5) as follows:

$$\begin{aligned} \frac{D\boldsymbol{\Omega}}{Dt} &= \frac{\partial \boldsymbol{\Omega}}{\partial t} + \mathbf{V} \cdot (\boldsymbol{\nabla}\boldsymbol{\Omega}) \\ &= \boldsymbol{\Omega} \cdot (\boldsymbol{\nabla}\mathbf{V}) + \nu \boldsymbol{\nabla}^2 \boldsymbol{\Omega} \end{aligned} \tag{2.6}$$

One can use either Equation (2.5) or Equation (2.6).

The term $\mathbf{V} \cdot (\boldsymbol{\nabla}\boldsymbol{\Omega})$ represents the rate of change due to convection of the fluid. The term $\boldsymbol{\Omega} \cdot (\boldsymbol{\nabla}\mathbf{V})$ represents the rate of deformation of the vortex lines and exists only in a three-dimensional flow. The stretching of the vortex lines concentrates vorticity and increases velocity fluctuations in the flow. The last term represents the rate of change due to molecular diffusion of vorticity. The set of Equations (2.2) to (2.5) or (2.6), with $\mathbf{V}(\mathbf{R}, t)$ and $\boldsymbol{\Omega}(\mathbf{R}, t)$ as basic dependent variables, replaces the set of Equations (2.1) and (2.2) in which $\mathbf{V}(\mathbf{R}, t)$ and $p(\mathbf{R}, t)$

are the basic dependent variables.

There are several reasons for using $\boldsymbol{\Omega}$ in the formulation of the problem. The first and perhaps the principal one is that the set of equations in terms of $\mathbf{V}$ and $\boldsymbol{\Omega}$ separate conveniently into two parts, each one constituting an entity by itself: a kinetic part which deals with the change of the vorticity field $\boldsymbol{\Omega}(\mathbf{R}, t)$ with time and a kinematic part which associates a velocity field $\mathbf{V}(\mathbf{R}, t)$ at any instant with the vorticity field $\boldsymbol{\Omega}(\mathbf{R}, t)$ at that instant. It will be shown that the separation of the problem into component parts permits an integral representation of the velocity field in terms of the vorticity field and the boundary conditions. The second one is that the use of the vorticity vector, which is intimately connected with viscosity effects, permits the computation of the whole velocity field $\mathbf{V}(\mathbf{R}, t)$ for an incompressible fluid to be confined to the viscous region only. The third one is that the circulation theory for the lift force suggests that the vorticity of the flow, which ultimately can be related to the circulation, is responsible for the force and moment exerted by the fluid on the solid.

2.2 Kinetics of the Vorticity Field

The kinetic aspect of the problem is concerned with the development of the vorticity field with time. This aspect, i.e., the rate of change of the vorticity field $\boldsymbol{\Omega}(\mathbf{R}, t)$ at a given location $\mathbf{R}$ of the flow field, is described by the vorticity transport Equation (2.5) or (2.6). For an inviscid fluid, $\nu = 0$, the last term in Equations (2.5) and (2.6) vanishes and the vorticity is convected with the fluid in the sense that the flux of vorticity, $\boldsymbol{\Omega} \cdot \mathbf{n}\, dS$ associated with each surface element moving with the fluid remains constant for all times. In an inviscid fluid, vorticity is a kinematic property of a given particle and, like matter, can neither be created nor destroyed, i.e., vortex lines are material lines [160, 161, 162]. Thus, it can undergo only convection and deformation. The last term in Equations (2.5) and (2.6) states that in a real fluid, however, in addition to being convected, the vorticity produced at a boundary diffuses as a consequence of viscous action. Changes in the flux of vorticity across a surface element that is moving with the fluid and is in the interior of the fluid domain takes place only by diffusion. Vorticity flux cannot be created in the interior of a fluid. This process determines the entire flow field which in turn controls the production of vorticity. According to Sarpkaya [70], "The discretized

representation (approximation) of these processes, particularly in flows where the distribution of vorticity is compact, constitutes the essence of the computational methods with vortices." The computational methods with vortices owe their existence to the vorticity equation and to the fact that the distribution of vorticity in real flows is often sufficiently compact for its idealization in terms of singular vortices imbedded in an otherwise irrotational domain. The higher the Reynolds number is, the more compact the regions of vorticity are.

The no-slip condition provides a mechanism for the generation of vorticity at the surface of a solid. The generation of vorticity at rigid boundaries and its subsequent decay have been the subject of much discussion. Lighthill [163] invoked the existence of vorticity sources in a region of falling pressure along the boundary and vorticity sinks in a following region of rising pressure. Batchelor [164] also noted that "vorticity cannot be created or destroyed in the interior of a homogeneous fluid under normal conditions, and is produced only at the boundaries," implying that the mechanism whereby vorticity is lost is by diffusion to the boundaries. For Batchelor, "normal conditions" excludes the merger of two streams with different velocities. Some of these statements are inconsistent with later observations.

Morton has revised and clarified all prior concepts regarding the generation and decay of vorticity. His conclusions will be summarized here since the understanding of where and how vorticity is generated (and lost) is of central importance for understanding the numerical scheme used in this work. According to Morton [165], any comprehensive treatment of the generation and decay of vorticity must take the following into account:

1. that vorticity generation results from tangential acceleration of a boundary, from tangential initiation of boundary motion and from tangential pressure gradients acting along the boundary;

2. that vorticity once generated cannot subsequently be lost by diffusion to boundaries;

3. that reversal of the sense of acceleration or of the sense of pressure gradient results in reversal of the sense of vorticity generated (vorticity sink, according to Lighthill's interpretation);

4. that walls play no direct role in the decay or loss of vorticity; and,

5. that vorticity decay results from cross-diffusion of two fluxes of opposite sense and takes place in the fluid interior.

In the case where the fluid is initially at rest and occupies an infinite domain bounded internally by a solid surface whose velocity rises suddenly at $t = 0$ to some finite value and remains steady thereafter, the vorticity is everywhere zero for $t < 0$. Since the vorticity flux in the interior of the fluid domain can change only as a consequence of viscous diffusion, the flow is irrotational at $t = 0$ everywhere except only at the solid surface. In general, this irrotational flow set up by the motion of the solid has a non-zero tangential velocity relative to the solid. A discontinuity in tangential velocity therefore results, at $t = 0$, due to the no-slip condition. This discontinuity in tangential velocity represents a *sheet of vorticity* over the surface of the solid.

For $t > 0$, the vorticity, which is concentrated at the boundaries at $t = 0$, spreads into the interior of the fluid domains by diffusion and shedding and, once there, can be rapidly transported far away from the boundaries by convection. As $t \to \infty$, a steady state distribution of vorticity may become established. If the Reynolds number is large the vorticity spreads only a short distance from the solid surface before being shed and then carried away with the fluid. *Thus there exists a large region of the fluid, ahead and to the side of the body, in which the fluid is free of vorticity.* Since Equation (2.5) is parabolic, with both $\mathbf{V}(\mathbf{R}, t)$ and $\boldsymbol{\Omega}(\mathbf{R}, t)$ known in the viscous region at any given time t, the rate of change of $\boldsymbol{\Omega}$ and hence the distribution of $\boldsymbol{\Omega}(\mathbf{R}, t)$ at a subsequent time, say $t + \Delta t$, can be computed using Equation (2.5). Consequently, if the kinematic relationship between $\mathbf{V}(\mathbf{R}, t)$ and $\boldsymbol{\Omega}(\mathbf{R}, t)$ is formulated in such a manner that the evaluation of $\mathbf{V}(\mathbf{R}, t)$ can be confined to the viscous region at each time step, then the entire solution, which follows the development of the vorticity with time, can also be confined to this relatively small viscous region. With the integral representation of the velocity field used in this thesis, this ability to confine the solution to the viscous region is indeed realizable.

The solution of real fluid-flow problems with vortex models forces one to think about the behavior of vortices in terms of viscous and inviscid concepts. Thus, it is necessary to summarize some of the major differences between the characteristics of vortices in viscous and inviscid fluids. In an inviscid incompressible fluid of uniform density, subjected to irrotational body forces, the circulation around any closed material curve is invariant with time (Kelvin's circu-

lation theorem, [160, 161, 162, 164]). This is a consequence of the fact that there is no diffusion and vorticity is transported solely by the convection of the fluid. In a viscous fluid, however, the circulation about a closed contour moving with the fluid depends on time. The only way to change the angular momentum of a fluid particle is to apply a moment to it, and this requires shear stresses. Shear stresses (and diffusion) are dependent on the existence of viscosity.. The rate of change of vorticity in a material volume is due solely to diffusion across the boundary of the volume. The appreciation of this difference is of importance in the determination of the vorticity generated by a body and the strength and position of the vorticity found in the wake.

2.3 Kinematics of the flow

The kinematic aspect of the problem is concerned with the relationship between the vorticity distribution and the velocity distribution at any given instant. The differential equations describing this relationship between $\mathbf{V}(\mathbf{R},t)$ and $\boldsymbol{\Omega}(\mathbf{R},t)$ are the continuity Equation (2.2) and the definition of vorticity, Equation (2.3), which for convenience are repeated here

$$\begin{aligned} \boldsymbol{\nabla}\cdot\mathbf{V} &= 0 \\ \boldsymbol{\nabla}\times\mathbf{V} &= \boldsymbol{\Omega} \end{aligned}$$

There is an analogy between these two equations and Maxwell's equations relating the magnetic field and the steady flow of electric current. Thus the well established techniques for magnetostatics may be utilized in treating the kinematic aspects of the incompressible flow problem under consideration. It must be emphasized, however, that although in magnetostatics the electric current is said to produce a magnetic field and in fluid dynamics the vorticity is customarily said to induce a velocity field, the relation between $\mathbf{V}(\mathbf{R},t)$ and $\boldsymbol{\Omega}(\mathbf{R},t)$ is in fact *purely kinematic. The two fields* $\mathbf{V}(\mathbf{R},t)$ *and* $\boldsymbol{\Omega}(\mathbf{R},t)$ *simply co-exist and the word "induce" does not imply a mechanical cause and effect.* The usual method of evaluating $\mathbf{V}(\mathbf{R},t)$ is to take the curl of Equation (2.3) and, by using Equation (2.2), obtain a vector Poisson's equation for $\mathbf{V}(\mathbf{R},t)$ in the form

$$\boldsymbol{\nabla}^2\mathbf{V} = -\boldsymbol{\nabla}\times\boldsymbol{\Omega} \tag{2.7}$$

The usual methods for the evaluation of $\mathbf{V}$ utilize a finite difference method to solve Equation (2.7). Since Poisson's equation is elliptic, the finite difference solution for $\mathbf{V}$ at a given point in the flow depends on the value of $\mathbf{V}$ at the neighboring points. It is therefore not possible to evaluate, with a finite difference scheme, the value of $\mathbf{V}$ explicitly, point by point, in the flow field.

Thompson [166] and Wu and Thompson [167] developed an integral representation for $\mathbf{V}(\mathbf{R},t)$ in the form

$$\mathbf{V}(\mathbf{R},t)=\frac{1}{4\pi}\int_V \frac{\boldsymbol{\nabla}_0\times\boldsymbol{\Omega}_0}{\|\mathbf{R}-\mathbf{R}_0\|_2}\,dV_0+\frac{1}{4\pi}\oint_S \frac{\mathbf{V}_0\left[(\mathbf{R}-\mathbf{R}_0)\cdot\mathbf{n}_0\right]}{\|\mathbf{R}-\mathbf{R}_0\|_2^3}\,dS_0+\frac{1}{4\pi}\oint_S \frac{\partial\mathbf{V}_0/\partial\mathbf{n}_0}{\|\mathbf{R}-\mathbf{R}_0\|_2}\,dS_0 \quad (2.8)$$

where the volume V is bounded by the surface S consisting of either a single closed surface or a closed outer surface and one or more closed inner surfaces, $\boldsymbol{\Omega}(\mathbf{R},t)$ is single-valued, finite, and has continuous first derivatives in V. The subscript "0" indicates that the variables, the differentiations, and the integrations are in the $\mathbf{R}_0$ space, i.e.,

$$\boldsymbol{\nabla}_0=\frac{\partial}{\partial X_0}\hat{\mathbf{I}}+\frac{\partial}{\partial Y_0}\hat{\mathbf{J}}+\frac{\partial}{\partial Z_0}\hat{\mathbf{K}},\qquad \boldsymbol{\Omega}_0=\boldsymbol{\Omega}(\mathbf{R}_0,t),\qquad dV_0=dX_0\;dY_0\;dY_0,\ \text{etc.}$$

Since Equation (2.7) is elliptic, the correct boundary condition to prescribe is either Dirichlet's (essential) or Neumann's (natural), or a linear combination of the two, over the entire boundary S. The use of Equation (2.8), however, requires both $\mathbf{V}$ and $\partial\mathbf{V}/\partial\mathbf{n}$ to be specified on S. For certain problems, it is possible to avoid this difficulty by introducing image vortices [169], or to use Green's functions [170]. Such procedures, however, are impractical for all but a few problems involving very simple boundary geometry. For a more general situation where the boundary S, or part of S, may be in the interior of the fluid domain, the expression obtained by Wu and Thompson in reference [168] is more convenient.

Wu and Thompson noted that, on the basis of Equation (2.2), the vector field $\mathbf{V}(\mathbf{R},t)$ is solenoidal and, therefore, a vector potential $\boldsymbol{\Psi}(\mathbf{R},t)$ exists such that

$$\mathbf{V}=\boldsymbol{\nabla}\times\boldsymbol{\Psi} \quad (2.9)$$

since the curl of any gradient vector is zero, the vector field $\boldsymbol{\Psi}(\mathbf{R},t)$ is indeterminate to the

extent of the gradient of a scalar function of position $\mathbf{R}$ and time t. Placing Equation (2.9) into Equation (2.3) yields

$$\begin{aligned} \boldsymbol{\Omega} &= \boldsymbol{\nabla} \times (\boldsymbol{\nabla} \times \boldsymbol{\Psi}) \\ &= \boldsymbol{\nabla} (\boldsymbol{\nabla} \cdot \boldsymbol{\Psi}) - \boldsymbol{\nabla}^2 \boldsymbol{\Psi} \end{aligned} \tag{2.10}$$

Green's theorem for vectors states that, if $\mathbf{P}$ and $\mathbf{Q}$ are single-valued and finite and have continuous second order derivatives, then

$$\begin{aligned} &\int_V \{\mathbf{P} \cdot [\boldsymbol{\nabla} \times (\boldsymbol{\nabla} \times \mathbf{Q})] - \mathbf{Q} \cdot [\boldsymbol{\nabla} \times (\boldsymbol{\nabla} \times \mathbf{P})]\} \, dV \\ = &\oint_S [\mathbf{Q} \times (\boldsymbol{\nabla} \times \mathbf{P}) - \mathbf{P} \times (\boldsymbol{\nabla} \times \mathbf{Q})] \cdot \mathbf{n} \, dS \end{aligned} \tag{2.11}$$

where the volume V is bounded by S which is a closed surface, or a closed outer surface and one or more closed inner surfaces, the latter enclosed by the former.

Let $\mathbf{P}$ be a principal solution of the equation $\boldsymbol{\nabla} \times (\boldsymbol{\nabla} \times \mathbf{P}) = \mathbf{0}$ [171], given by

$$\mathbf{P} = \boldsymbol{\nabla} \left(\frac{1}{R'} \right) \times \mathbf{a} = \boldsymbol{\nabla} \times \left(\frac{\mathbf{a}}{R'} \right) \tag{2.12}$$

where $\mathbf{a}$ is a constant unit vector,

$$R' = \|\mathbf{R}_0 - \mathbf{R}\|_2 \tag{2.13}$$

and the following vector identity was used

$$\boldsymbol{\nabla} \times (f\mathbf{F}) = f \ (\boldsymbol{\nabla} \times \mathbf{F}) + \boldsymbol{\nabla} f \times \mathbf{F}$$

Let

$$\mathbf{Q} = \boldsymbol{\Psi} \tag{2.14}$$

It can be shown that, for $R' \neq 0$,

$$\boldsymbol{\nabla} \times \mathbf{P} = \boldsymbol{\nabla} \left[\mathbf{a} \cdot \boldsymbol{\nabla} \left(\frac{1}{R'} \right) \right] \tag{2.15}$$

and

$$\boldsymbol{\nabla} \times (\boldsymbol{\nabla} \times \mathbf{P}) = \boldsymbol{\nabla} \times \left\{ \boldsymbol{\nabla} \left[\mathbf{a} \cdot \boldsymbol{\nabla} \left(\frac{1}{R'} \right) \right] \right\} = \mathbf{0} \tag{2.16}$$

Consider V to be bounded internally by S_1, and externally by S_2, S_1 being a small spherical surface of radius ϵ with its center at $\mathbf{R}_0$. Substituting Equations (2.9), (2.10), and (2.12)-(2.16) into Equation (2.11), we obtain

$$\begin{aligned} \int_V \left[\boldsymbol{\nabla} \left(\frac{1}{R'} \right) \times \mathbf{a} \right] \cdot \boldsymbol{\Omega} \, dV &= \oint_{S_1+S_2} \left\{ \boldsymbol{\Psi} \times \boldsymbol{\nabla} \left[\mathbf{a} \cdot \nabla \left(\frac{1}{R'} \right) \right] \right\} \cdot \mathbf{n} \, dS \\ &- \oint_{S_1+S_2} \left\{ \left[\boldsymbol{\nabla} \left(\frac{1}{R'} \right) \times \mathbf{a} \right] \times \mathbf{V} \right\} \cdot \mathbf{n} \, dS \end{aligned} \tag{2.17}$$

Equation (2.17) can be rewritten as

$$\begin{aligned} \int_V \mathbf{a} \cdot \left[\boldsymbol{\Omega} \times \boldsymbol{\nabla} \left(\frac{1}{R'} \right) \right] \, dV &= \oint_{S_1+S_2} \left\{ \left[\mathbf{a} \cdot \boldsymbol{\nabla} \left(\frac{1}{R'} \right) \right] \mathbf{V} \right\} \cdot \mathbf{n} \, dS \\ &- \oint_{S_1+S_2} \mathbf{a} \cdot \left[(\mathbf{V} \times \mathbf{n}) \times \boldsymbol{\nabla} \left(\frac{1}{R'} \right) \right] \, dS \end{aligned} \tag{2.18}$$

On S_1 as $\epsilon \to 0$, one has

$$\boldsymbol{\nabla} \left(\frac{1}{R'} \right) \to \frac{\mathbf{n}}{\epsilon^2}$$

Consequently, as $\epsilon \to 0$, one has

$$\begin{aligned} &\oint_{S_1} \left\{ \left[\mathbf{a} \cdot \boldsymbol{\nabla} \left(\frac{1}{R'} \right) \right] \mathbf{V} \right\} \cdot \mathbf{n} \, dS - \oint_{S_1} \mathbf{a} \cdot \left[(\mathbf{V} \times \mathbf{n}) \times \boldsymbol{\nabla} \left(\frac{1}{R'} \right) \right] \, dS \\ \to \quad &\oint \left\{ \mathbf{a} \cdot [\mathbf{n} \, (\mathbf{V} \cdot \mathbf{n})] + \mathbf{a} \cdot [(\mathbf{V} \times \mathbf{n}) \times \mathbf{n}] \right\} d\varpi = 4\pi \mathbf{a} \cdot \mathbf{V} \, (\mathbf{R}_0) \end{aligned} \tag{2.19}$$

where ϖ is the solid angle subtended by dS at $\mathbf{R}_0$.

Noting that the direction of $\mathbf{a}$ is arbitrary, one obtains from Equations (2.18) and (2.19), upon interchanging $\mathbf{R}_0$ and $\mathbf{R}$:

$$\mathbf{V} \, (\mathbf{R}, t) = \frac{1}{4\pi} \int_V \boldsymbol{\Omega}_0 \times \boldsymbol{\nabla} \left(\frac{1}{R'} \right) \, dV_0 - \frac{1}{4\pi} \oint_S (\mathbf{V}_0 \cdot \mathbf{n}_0) \, \boldsymbol{\nabla} \left(\frac{1}{R'} \right) \, dS_0$$

$$+ \quad \frac{1}{4\pi} \oint_S (\mathbf{V}_0 \times \mathbf{n}_0) \times \boldsymbol{\nabla} \left(\frac{1}{R'} \right) \, dS_0 \tag{2.20}$$

The volume integral over the interior of S_1 goes to zero as $\epsilon \to 0$. Thus in Equation (2.20) V is the entire volume bounded by S.

A similar expression for two-dimensional flow problems can be obtained by replacing $1/R'$ by $\ln\left(1/R'\right)$. In fact, Equation (2.20) can be written in the general form

$$\begin{aligned} \mathbf{V}(\mathbf{R}, t) &= -\frac{1}{A} \int_V \frac{\boldsymbol{\Omega}_0 \times (\mathbf{R}_0 - \mathbf{R})}{\|\mathbf{R}_0 - \mathbf{R}\|_2^d} \, dV_0 - \frac{1}{A} \oint_S \frac{(\mathbf{V}_0 \cdot \mathbf{n}_0)(\mathbf{R}_0 - \mathbf{R})}{\|\mathbf{R}_0 - \mathbf{R}\|_2^d} \, dS_0 \\ &+ \frac{1}{A} \oint_S \frac{(\mathbf{V}_0 \times \mathbf{n}_0) \times (\mathbf{R}_0 - \mathbf{R})}{\|\mathbf{R}_0 - \mathbf{R}\|_2^d} \, dS_0 + \mathbf{B} \end{aligned} \tag{2.21}$$

where in three-dimensions $A = 4\pi$ and $d = 3$, and in two-dimensions $A = 2\pi$ and $d = 2$. The vector $\mathbf{B}$ vanishes for flows in the interior of S and is equal to $\mathbf{V}_\infty$, the constant free-stream velocity at infinity, for flows in the exterior of S.

The integral representation of $\mathbf{V}(\mathbf{R}, t)$ in terms of $\boldsymbol{\Omega}$, Equation (2.21), is an extension of the well-known Biot-Savart law which was found experimentally by Biot and Savart in 1820 in connection with the determination of the magnetic field intensity (corresponding to $\|\mathbf{V}\|_2$) induced by a flow of electric current (corresponding to $\|\boldsymbol{\Omega}\|_2$) and was established analytically by Ampere in 1826. The contribution of the vorticity outside the region V is taken into account by the two surface integrals in Equation (2.21). If S represents the surface of a solid on which $\mathbf{V} = \mathbf{0}$, then Equation (2.21) reduces to (see, e.g., Karamcheti [160], Sommerfeld [161], and Batchelor [164])

$$\mathbf{V}(\mathbf{R}, t) = \frac{1}{A} \int_V \frac{\boldsymbol{\Omega}(\mathbf{R}_0, t) \times (\mathbf{R} - \mathbf{R}_0)}{\|\mathbf{R} - \mathbf{R}_0\|_2^d} \, dV(\mathbf{R}_0) + \mathbf{B} \tag{2.22}$$

It is important to emphasize that the integrand in the volume integral is zero wherever $\boldsymbol{\Omega}$ vanishes. Thus the region where the flow is irrotational does not contribute to $\mathbf{V}$ anywhere. $\mathbf{V}$ can be evaluated explicitly at each point, i.e., independently of the evaluation of $\mathbf{V}$ at neighboring points. As a consequence of this feature, which is absent in finite difference methods, in the kinematic part of the problem the evaluation of $\mathbf{V}$ can be confined to the viscous region. This ability to confine the study to the viscous region only results not from any simplifications

of the Navier-Stokes equations (as in the case of Boundary Layer theory) but from the use of the integral representation which permits the velocity distribution to be computed for the inviscid region as well as for the viscous region based on the distribution of vorticity in the viscous region only. The velocity in the inviscid region varies from point to point since each different value of $\mathbf{R}$ in the integrand of Equation (2.22) gives a different value for the integral. For external flow problems, the imposed boundary conditions at infinity are contained implicitly in Equation (2.22). Thus, for example, for the flow past a solid body, Equation (2.22) gives $\mathbf{V} \to \mathbf{V}_\infty$ as $\mathbf{R} \to \infty$.

For three-dimensional flows, taking into account that

$$\boldsymbol{\nabla}_{\mathbf{R}} \frac{1}{\|\mathbf{R} - \mathbf{R}_0\|_2} = -\frac{\mathbf{R} - \mathbf{R}_0}{\|\mathbf{R} - \mathbf{R}_0\|_2^3} \tag{2.23}$$

we can write the velocity field associated with a bounded distribution of vorticity as

$$\mathbf{V}(\mathbf{R}, t) = \frac{1}{4\pi} \int_V \frac{\boldsymbol{\Omega}(\mathbf{R}_0, t) \times (\mathbf{R} - \mathbf{R}_0)}{\|\mathbf{R} - \mathbf{R}_0\|_2^3} \, dV(\mathbf{R}_0) \tag{2.24}$$

$$= -\frac{1}{4\pi} \int_V \boldsymbol{\Omega}(\mathbf{R}_0, t) \times \boldsymbol{\nabla}_{\mathbf{R}} \frac{1}{\|\mathbf{R} - \mathbf{R}_0\|_2} \, dV(\mathbf{R}_0) \tag{2.25}$$

It follows from Equation (2.2) [160, 161] that this expressions can also be obtained by inverting Equation (2.3) and making use of the fact that the fluid is incompressible.

2.4 Vortex Sheets

Surfaces on which the vorticity is infinite are kinematically possible and do not necessarily violate dynamical properties. These structures, called vortex sheets, are surfaces across which the tangential component of the velocity field is discontinuous. They can be introduced formally as surfaces of discontinuity or imagined to come from a limiting processes in which the vorticity is confined to a thin, surface-like region of thickness ϵ, and the limit is taken as $\epsilon \to 0$ while the magnitude of the vorticity Ω goes to infinity in such a way that $\epsilon \, \Omega \to \gamma$, where γ is finite and is in general a function of the position on the surface.

We can express the vorticity in a vortex sheet in the form

$$\boldsymbol{\Omega} = \boldsymbol{\gamma}\ \delta(n) \tag{2.26}$$

where $\boldsymbol{\gamma} \cdot \mathbf{n} = 0$, $\gamma = \|\boldsymbol{\gamma}\|_2$, n is the distance along the normal to the sheet $\mathbf{n}$, and $\delta(n)$ is the Dirac delta generalized function. A sheet vortex line is defined as a curve such that $\boldsymbol{\gamma}$ is tangent to it at every point on the sheet. The solenoidal property of vorticity (i.e., $\boldsymbol{\Omega} = \boldsymbol{\nabla} \times \mathbf{V}$) gives

$$\boldsymbol{\nabla}_{VS} \cdot \boldsymbol{\gamma} = 0 \tag{2.27}$$

where $\boldsymbol{\nabla}_{VS}$ is a two-dimensional operator on the surface of the vortex sheet. It is a consequence of Equation (2.27) that vortex lines in the vortex sheet are either closed or end on the boundaries [160, 161, 162, 164].

The velocity field $\mathbf{V}(\mathbf{R}, t)$ associated with a vortex sheet follows from the integral expression (2.24). The substitution of Equation (2.26) into this equation converts the volume integral into a surface integral over the vortex sheet S_{VS}. We obtain

$$\mathbf{V}(\mathbf{R}, t) = \frac{1}{4\pi} \int\limits_{S_{VS}} \frac{\boldsymbol{\gamma}(\mathbf{R}_0, t) \times (\mathbf{R} - \mathbf{R}_0)}{\|\mathbf{R} - \mathbf{R}_0\|_2^3}\ dS(\mathbf{R}_0) \tag{2.28}$$

where $\mathbf{R}_0$ is a position vector on the sheet and $dS(\mathbf{R}_0)$ is the element of surface (Figure 2-1). The velocity field defined by Equation (2.28) is finite when the field point $\mathbf{R}$ is off the vortex sheet. We now will consider the behavior of this velocity field as a point P with position vector $\mathbf{R}_P$ approaches a point Q located on the sheet with position vector $\mathbf{R}_Q$, see Figure 2-2. To this end we rewrite Equation (2.28) as follows

$$\begin{aligned}
\mathbf{V}(\mathbf{R}_P, t) &= \frac{1}{4\pi} \int\limits_{S_{VS}} \frac{\boldsymbol{\gamma}(\mathbf{R}_0, t) \times (\mathbf{R}_P - \mathbf{R}_0)}{\|\mathbf{R}_P - \mathbf{R}_0\|_2^3}\ dS(\mathbf{R}_0) \\
&+ \frac{1}{4\pi} \int\limits_{S_{VS}} \frac{\boldsymbol{\gamma}(\mathbf{R}_Q, t) \times (\mathbf{R}_P - \mathbf{R}_0)}{\|\mathbf{R}_P - \mathbf{R}_0\|_2^3}\ dS(\mathbf{R}_0) \\
&- \frac{1}{4\pi} \int\limits_{S_{VS}} \frac{\boldsymbol{\gamma}(\mathbf{R}_Q, t) \times (\mathbf{R}_P - \mathbf{R}_0)}{\|\mathbf{R}_P - \mathbf{R}_0\|_2^3}\ dS(\mathbf{R}_0)
\end{aligned}$$

or

$$\begin{aligned}\mathbf{V}(\mathbf{R}_P,t) &= \frac{1}{4\pi}\boldsymbol{\gamma}(\mathbf{R}_Q,t)\times\int\limits_{S_{VS}}\frac{\mathbf{R}_{0P}}{R_{0P}^3}\,dS(\mathbf{R}_0)\\ &+ \frac{1}{4\pi}\int\limits_{S_{VS}}\left[\boldsymbol{\gamma}(\mathbf{R}_0,t)-\boldsymbol{\gamma}(\mathbf{R}_Q,t)\right]\times\frac{\mathbf{R}_{0P}}{R_{0P}^3}\,dS(\mathbf{R}_0)\end{aligned} \tag{2.29}$$

where $\mathbf{R}_{0P}=\mathbf{R}_P-\mathbf{R}_0$ and $R_{0P}=\|\mathbf{R}_P-\mathbf{R}_0\|_2$. It can be shown that the second term on the right-hand side of Equation (2.29) has a unique limit as $P\to Q$ which is given by

$$\lim_{P\to Q}\frac{1}{4\pi}\int\limits_{S_{VS}}\left[\boldsymbol{\gamma}(\mathbf{R}_0,t)-\boldsymbol{\gamma}(\mathbf{R}_Q,t)\right]\times\frac{\mathbf{R}_{0P}}{R_{0P}^3}\,dS(\mathbf{R}_0)=\frac{1}{4\pi}\int\limits_{S_{VS}}\frac{\boldsymbol{\gamma}(\mathbf{R}_0,t)\times(\mathbf{R}_Q-\mathbf{R}_0)}{\|\mathbf{R}_Q-\mathbf{R}_0\|_2^3}\,dS(\mathbf{R}_0) \tag{2.30}$$

where the integral on the right-hand side must be considered a principal value integral analogous to the Cauchy principal value, with the vorticity in an infinitesimal circle centered at Q excluded from the integral. The limit of the first term on the right-hand side of Equation (2.29) is finite but discontinuous; its value depends on the side from which the vortex sheet is approached:

$$\lim_{P_1\to Q}\int\limits_{S_{VS}}\frac{\mathbf{R}_{0P_1}}{R_{0P_1}^3}\,dS(\mathbf{R}_0)-\lim_{P_2\to Q}\int\limits_{S_{VS}}\frac{\mathbf{R}_{0P_2}}{R_{0P_2}^3}\,dS(\mathbf{R}_0)=4\pi\,\mathbf{n}(\mathbf{R}_Q,t) \tag{2.31}$$

where the normal $\mathbf{n}$ at point Q is defined from side 2 into side 1. These results can be put into the following form

$$\begin{aligned}\lim_{P\to Q}\mathbf{V}(\mathbf{R}_P,t) &= \pm\frac{1}{2}\boldsymbol{\gamma}(\mathbf{R}_Q,t)\times\mathbf{n}(\mathbf{R}_Q,t)\\ &+ \frac{1}{4\pi}\int\limits_{S_{VS}}\frac{\boldsymbol{\gamma}(\mathbf{R}_0,t)\times(\mathbf{R}_Q-\mathbf{R}_0)}{\|\mathbf{R}_Q-\mathbf{R}_0\|_2^3}\,dS(\mathbf{R}_0)\end{aligned} \tag{2.32}$$

the sign in Equation (2.32) is positive if P approaches Q from the side into which $\mathbf{n}$ points. Thus, the velocity associated with a vortex sheet is finite but has a simple jump in the tangential component across the sheet. The normal component of the velocity is continuous. The jump $\mathbf{V}_2^1$ in the tangential velocity (Figure 2-3) is given by

$$\mathbf{V}_2^1 = \mathbf{V}(\mathbf{R}_1,t)-\mathbf{V}(\mathbf{R}_2,t)$$

$$= \quad \boldsymbol{\gamma} \times \mathbf{n} \tag{2.33}$$

Moreover, by making use of the Euler equation for conservation of momentum in an ideal flow the following results can be proven (see, e.g., Saffman [172])

$$p_2 = p_1 \tag{2.34}$$

$$\mathbf{V}(\mathbf{R}_0, t) \cdot \mathbf{n} = \mathbf{V}(\mathbf{R}_2, t) \cdot \mathbf{n} = \mathbf{V}(\mathbf{R}_1, t) \cdot \mathbf{n} \tag{2.35}$$

these results show that the pressure is continuous across the vortex sheet and the sheet moves with the fluid.

2.5 Line Vortices

A line vortex is a singularity in which infinite vorticity is concentrated in a single curve in space, such that the circulation around a closed circuit threaded once by the line vortex is finite. Its strength, Γ, is the circulation around it, which is independent of the particular circuit when the line vortex threads it once (Figure 2-4). Line vortices are the result of a limiting process in which a vortex filament of infinitesimal area and finite strength is contracted to a curve, the strength being kept constant. Let this curve be defined parametrically by the following vector equation:

$$\mathbf{R}_0 = \mathbf{R}_0(s) \tag{2.36}$$

When the parameter s is taken as the arc length measured from some fixed point on the curve, we have the Frenet-Serret formulae [173]

$$\frac{d}{ds}\mathbf{R}_0 = \hat{\mathbf{t}}, \quad \frac{d}{ds}\hat{\mathbf{t}} = \hat{\mathbf{n}}, \quad \frac{d}{ds}\hat{\mathbf{n}} = -\hat{\mathbf{t}} + \tau\hat{\mathbf{b}}, \quad \frac{d}{ds}\hat{\mathbf{b}} = -\tau\hat{\mathbf{n}} \tag{2.37}$$

where $\hat{\mathbf{t}} = \hat{\mathbf{t}}(s)$ is the unit tangent vector to the curve $\mathbf{R}_0 = \mathbf{R}_0(s)$; $\hat{\mathbf{n}} = \hat{\mathbf{n}}(s)$ is a unit vector which is normal to the curve and is called the principal normal to the curve; and, $\hat{\mathbf{b}} = \hat{\mathbf{b}}(s)$ is a unit vector perpendicular to the plane of $\hat{\mathbf{t}}$ and $\hat{\mathbf{n}}$ and such that $\hat{\mathbf{b}} = \hat{\mathbf{t}} \times \hat{\mathbf{n}}$ called the binormal vector. (s) is the curvature, and $\tau(s)$ is the torsion. The triad $\left(\hat{\mathbf{t}}, \hat{\mathbf{n}}, \hat{\mathbf{b}}\right)$ forms a local

orthogonal coordinate system at any specified point of the curve.

As in the case of a vortex sheet, the vorticity can formally be expressed by making use of the Dirac delta generalized function and the coordinate system introduced above as follows

$$\boldsymbol{\Omega} = \Gamma \ \delta(n) \ \ \delta(b) \ \ \hat{\mathbf{t}}(s) \tag{2.38}$$

where n and b denote co-ordinates in the normal and binormal direction. Substituting Equation (2.38) into Equation (2.24) and taking into account that $dV(\mathbf{R}_0) = ds\ dn\ db$, we obtain the Biot-Savart law

$$\mathbf{V}(\mathbf{R}, t) = \frac{\Gamma}{4\pi} \oint \frac{\hat{\mathbf{t}}(s) \times [\mathbf{R} - \mathbf{R}_0(s)]}{\|\mathbf{R} - \mathbf{R}_0(s)\|_2^3} \ ds = \frac{\Gamma}{4\pi} \boldsymbol{\nabla} \times \oint \frac{d\hat{\mathbf{t}}(s)}{\|\mathbf{R} - \mathbf{R}_0(s)\|_2} \tag{2.39}$$

for the velocity field $\mathbf{V}(\mathbf{R}, t)$ associated with a line vortex of strength Γ along the closed curve $\mathbf{R}_0(s)$. The expression for the velocity field associated with a bounded distribution of vorticity, Equation (2.24), and hence the Biot-Savart law, Equation (2.39), can be applied to an infinitely long line vortex, because the curve can be imagined closed by a large semi-circle of radius R_∞, and is found immediately from Equation (2.39) that the contribution from this portion is $O\left(\frac{1}{R_\infty}\right)$ which approaches zero as $R_\infty \to \infty$. The special case of the infinitely long straight line vortex (the rectilinear line vortex) is important in the development of this work. Equation (2.39) yields a logarithmically infinite self-induced velocity (Batchelor [164] and Saffman [172]) if the filament is curved, and zero self-induced velocity if it is straight, i.e., a line vortex. There are two additional difficulties with the Biot-Savart approach even for two-dimensional flow simulations with line vortices. First, the vortex filaments are singularities and, therefore, create large velocities and/or critical velocity differences in their neighborhood. This can cause instabilities and physically impossible sheet crossings along and near the edges of the sheet. The second difficulty with the Biot-Savart law is concerned with the CPU per time-step. The number of operations required for the velocity-field calculation is proportional to N^2 where N is the number of vortices. Thus, the CPU time increases significantly as more vortices are added [70].

2.5.1 Infinitely Long Straight Line Vortex

We now consider an infinitely long straight line vortex of strength Γ (Figure 2-5). To calculate the velocity field associated with this singularity we choose the origin of coordinates at some point on the line vortex. Then, according to Equation (2.39), the velocity field $\mathbf{V}(\mathbf{R},t)$ at a field point $\mathbf{R}$ is given by

$$\begin{aligned}\mathbf{V}(\mathbf{R},t) &= \frac{\Gamma}{4\pi}\int_{-\infty}^{+\infty}\frac{\hat{\mathbf{t}}(s)\times[\mathbf{R}-\mathbf{R}_0(s)]}{\|\mathbf{R}-\mathbf{R}_0(s)\|_2^3}\,ds \\ &= \frac{\Gamma}{4\pi}\int_{-\infty}^{+\infty}\frac{d\mathbf{R}_0(s)\times[\mathbf{R}-\mathbf{R}_0(s)]}{\|\mathbf{R}-\mathbf{R}_0(s)\|_2^3}\end{aligned} \tag{2.40}$$

where $d\mathbf{R}_0(s)=\hat{\mathbf{t}}(s)\;ds$ is an element of the filament at $\mathbf{R}_0(s)$. We denote $\mathbf{R}-\mathbf{R}_0(s)$ by $\mathbf{R}_1(s)$ and the direction (which is constant) of $d\mathbf{R}_0(s)\times[\mathbf{R}-\mathbf{R}_0(s)]=d\mathbf{R}_0(s)\times\mathbf{R}_1(s)$ by $\hat{\mathbf{e}}$ (see Figure 2-5). If $\theta(s)$ is the angle measured from $d\mathbf{R}_0(s)$ to $\mathbf{R}_1(s)$ (such that $\theta(s)\to 0$ as $s\to-\infty$ and $\theta(s)\to\pi$ as $s\to+\infty$), we have

$$\begin{aligned}d\mathbf{R}_0(s)\times\mathbf{R}_1(s) &= \|d\mathbf{R}_0(s)\|_2\;\|\mathbf{R}_1(s)\|_2\sin[\theta(s)]\;\hat{\mathbf{e}} \\ &= ds\;R_1(s)\;\sin[\theta(s)]\;\hat{\mathbf{e}}\end{aligned}$$

and Equation (2.40) becomes

$$\begin{aligned}\mathbf{V}(\mathbf{R},t) &= \frac{\Gamma}{4\pi}\int_{-\infty}^{+\infty}\frac{ds\;R_1(s)\;\sin[\theta(s)]\;\hat{\mathbf{e}}}{[R_1(s)]^3} \\ &= \hat{\mathbf{e}}\frac{\Gamma}{4\pi}\int_{-\infty}^{+\infty}\frac{\sin[\theta(s)]}{[R_1(s)]^2}ds\end{aligned} \tag{2.41}$$

since, as we noted before, $\hat{\mathbf{e}}$ is a constant vector.

Now let us denote by h the normal distance from the field point $\mathbf{R}$ to the line vortex and let $\mathbf{R}_0(s)$ denote the point of intersection with the vortex line of the normal to it from the field point (Figure 2-5). Then, we have

$$\|\mathbf{R}_1(s)\|_2 = R_1(s)$$

$$
\begin{aligned}
&= h \text{ cosec } \theta \\
\|\mathbf{R}_0(s_1)\|_2 - \|\mathbf{R}_0(s)\|_2 &= R_0(s_1) - R_0(s) \\
&= h \cot\theta \\
\|d\mathbf{R}_0(s)\|_2 &= ds \\
&= h \text{ cosec}^2\theta \, d\theta
\end{aligned}
$$

and then,

$$
\begin{aligned}
\int_{-\infty}^{+\infty} \frac{\sin[\theta(s)]}{[R_1(s)]^2} ds &= \int_0^{\pi} \frac{\sin\theta \; h \text{ cosec}^2\theta}{h^2 \text{ cosec}^2\theta} \, d\theta \qquad (2.42) \\
&= \frac{1}{h} \int_0^{\pi} \sin\theta \, d\theta \\
&= \frac{2}{h} \qquad (2.43)
\end{aligned}
$$

Hence, substituting Equation (2.43) into Equation (2.41) we obtain the following expression for the velocity field associated with an infinitely long straight line vortex of strength Γ:

$$
\mathbf{V}(\mathbf{R}, t) = \frac{\Gamma}{2\pi h} \hat{\mathbf{e}} \qquad (2.44)
$$

We can conclude that the motion is two-dimensional, the plane of motion being normal to the line vortex. The streamlines of the associated velocity field are circles with their center on the line vortex.

2.5.2 Finite Segment of a Straight Line Vortex

We now consider the velocity field associated with a finite segment of a straight line vortex of strength Γ. In order to evaluate it we make use of Equation (2.42) in which we change the limits of integration as follows (Figure 2-6):

$$
0 \to \theta_1, \quad \pi \to \theta_2
$$

then we obtain

$$\frac{1}{h}\int_{\theta_1}^{\theta_2}\sin(\theta)\ d\theta = \frac{1}{h}\left(\cos\theta_1 - \cos\theta_2\right) \tag{2.45}$$

Substituting Equation (2.45) into Equation (2.41) we obtain the following expression for the velocity field associated with a finite segment of a straight line vortex of strength Γ:

$$\mathbf{V}(\mathbf{R},t) = \frac{\Gamma}{4\pi h}\left(\cos\theta_1 - \cos\theta_2\right)\ \hat{\mathbf{e}} \tag{2.46}$$

Equation (2.46) can be rewritten in a more convenient form for programming as follows (see Figure 2-6):

$$\begin{aligned}
\mathbf{L}\times\mathbf{r}_1 &= \|\mathbf{L}\|_2\,\|\mathbf{r}_1\|_2\sin\theta_1\ \hat{\mathbf{e}} = \|\mathbf{L}\|_2\ h\ \hat{\mathbf{e}} \\
\|\mathbf{L}\times\mathbf{r}_1\|_2 &= \|\mathbf{L}\|_2\,\|\mathbf{r}_1\|_2\sin\theta_1 = \|\mathbf{L}\|_2\,h
\end{aligned}$$

$$h = \frac{\|\mathbf{L}\times\mathbf{r}_1\|_2}{\|\mathbf{L}\|_2}, \quad \hat{\mathbf{e}} = \frac{\mathbf{L}\times\mathbf{r}_1}{\|\mathbf{L}\times\mathbf{r}_1\|_2}$$

$$\begin{aligned}
\mathbf{L}\cdot\mathbf{r}_1 &= \|\mathbf{L}\|_2\,\|\mathbf{r}_1\|_2\cos\theta_1 \qquad \cos\theta_1 = \frac{\mathbf{L}\cdot\mathbf{r}_1}{\|\mathbf{L}\|_2\,\|\mathbf{r}_1\|_2} \\
\mathbf{L}\cdot\mathbf{r}_2 &= \|\mathbf{L}\|_2\,\|\mathbf{r}_2\|_2\cos\theta_2 \qquad \cos\theta_2 = \frac{\mathbf{L}\cdot\mathbf{r}_2}{\|\mathbf{L}\|_2\,\|\mathbf{r}_2\|_2}
\end{aligned}$$

$$\begin{aligned}
\mathbf{V}(\mathbf{R},t) &= \frac{\Gamma}{4\pi}\frac{1}{\dfrac{\|\mathbf{L}\times\mathbf{r}_1\|_2}{\|\mathbf{L}\|_2}}\left(\frac{\mathbf{L}\cdot\mathbf{r}_1}{\|\mathbf{L}\|_2\,\|\mathbf{r}_1\|_2} - \frac{\mathbf{L}\cdot\mathbf{r}_2}{\|\mathbf{L}\|_2\,\|\mathbf{r}_2\|_2}\right)\frac{\mathbf{L}\times\mathbf{r}_1}{\|\mathbf{L}\times\mathbf{r}_1\|_2} \\
&= \frac{\Gamma}{4\pi}\frac{\mathbf{L}\times\mathbf{r}_1}{\|\mathbf{L}\times\mathbf{r}_1\|_2^2}\left(\frac{\mathbf{L}\cdot\mathbf{r}_1}{\|\mathbf{r}_1\|_2} - \frac{\mathbf{L}\cdot\mathbf{r}_2}{\|\mathbf{r}_2\|_2}\right) \\
&= \frac{\Gamma}{4\pi}\frac{\mathbf{L}\times\mathbf{r}_1}{\|\mathbf{L}\times\mathbf{r}_1\|_2^2}\left[\mathbf{L}\cdot\left(\frac{\mathbf{r}_1}{\|\mathbf{r}_1\|_2} - \frac{\mathbf{r}_2}{\|\mathbf{r}_2\|_2}\right)\right]
\end{aligned}$$

$$\hat{\mathbf{e}}_1 = \frac{\mathbf{r}_1}{\|\mathbf{r}_1\|_2}, \text{ and } \hat{\mathbf{e}}_2 = \frac{\mathbf{r}_2}{\|\mathbf{r}_2\|_2}$$

$$\mathbf{V}(\mathbf{R},t) = \frac{\Gamma}{4\pi}\frac{\mathbf{L}\times\mathbf{r}_1}{\|\mathbf{L}\times\mathbf{r}_1\|_2^2}\left[\mathbf{L}\cdot(\hat{\mathbf{e}}_1 - \hat{\mathbf{e}}_2)\right] \tag{2.47}$$

2.6 Vortex Sheets and Viscous Boundary Layers

In all real high-Reynolds-number flows a boundary layer develops next to the surface of the body. Sufficient vorticity is present in this layer to change the fluid velocity so that the no-slip condition is satisfied on the body surface. The action of viscosity is to cause the vorticity in this layer to diffuse normal to the surface [165], resulting in the familiar viscous boundary layer. The vorticity itself is the product of the dynamic behavior of the outer flow and the rate of vorticity production in the boundary layer is directly related to the pressure gradient along the surface. Traditionally a high Reynolds number flow is usually regarded as comprising a large irrotational outer flow, separated from the body surface by a thin but highly rotational layer. These two regions, with different characteristics, are usually treated separately when the problem is approached analytically, with suitable matching conditions [174].

Suppose now that we were able to increase the Reynolds number indefinitely. In the limit, due to progressive reduction of viscous diffusion, the boundary layer will approach infinitesimal thickness. Thus, as the Reynolds number approaches infinity, the body surface will be covered with an infinitely thin vortex sheet of strength γ. For a body at rest the fluid velocity will change discontinuously from zero beneath the sheet on the body surface to V parallel to the surface just outside the sheet. Leaving aside the complications connected with instabilities of boundary layers at high Reynolds numbers, we see that inviscid potential flows can be thought of as a special type of infinite-Reynolds-number flow. In this sense the surface vorticity model accurately approximates the physical reality of a very large Reynolds number (but fully attached) flow and it is therefore the most natural of all numerical methods for potential flow analysis. Furthermore, it is also possible to introduce models to simulate viscous diffusion [175, 176], so that we may relax the present constraint of infinite Reynolds number. The surface vorticity method, unlike the source panel method, thus offers special attractions as a route towards the simulation of real fluid flows because the model truly reflects the physical reality.

2.7 Vorticity and Kutta Condition for Unsteady Flows

The Kutta condition for unsteady flows has been the subject of much discussion. Giesing [177] suggested that a simple statement of the Kutta condition for steady as well as for unsteady flows is that the velocities on the upper and lower surfaces at the trailing edges must be equal in magnitude but opposite in the tangential direction. He applied this condition both to bodies with nonzero angles at the trailing edge and to bodies with cusped trailing edges. Kármán and Sears [12] ended up with the condition, for a flat plate in unsteady flow, that the velocity on the upper and the lower surfaces differed by an amount equal to the shed vorticity. Van de Vooren and Van de Vel [178] found that an infinite velocity difference was allowable in unsteady flows. Katz and Maskew [96] noted that along the trailing edges of the wings the velocity has to be limited in order to fix the rear stagnation point (i.e. $\mathbf{V} < \infty$ at trailing edges). In this thesis, in order to satisfy the Kutta condition, we force the pressures to be finite and the difference between the pressures on the upper and lower surfaces to be zero along the edges of the wing. This forces the flow to leave the trailing edges and tips smoothly but with vorticity in general.

The unsteady Kutta condition requires that, in order for the pressure difference to vanish along the edges where wakes are attached, the vorticity created along the edges must be convected with the flow. We convect the vortex segments along the trailing edges and tips away from the wing at the local particle velocity; this process is called vorticity shedding. As this shed vorticity convects away from the wing at the local particle velocity, it forms the wakes. For an inviscid flow, this procedure eliminates discontinuities in the pressure and, therefore, renders the wakes force-free.

2.8 The Kelvin-Helmholtz Theorems and Spatial Conservation of Vorticity

We consider now the circulation around a closed material line C, which is given by:

$$\Gamma = \oint_{C(t)} \mathbf{V} \cdot d\mathbf{R} \tag{2.48}$$

Its rate of change $\dfrac{D\Gamma}{Dt}$ can be calculated as follows,

$$\frac{D\Gamma}{Dt} = \frac{D}{Dt} \oint\limits_{C(t)} \mathbf{V} \cdot d\mathbf{R} = \oint\limits_{C(t)} \frac{D\mathbf{V}}{Dt} \cdot d\mathbf{R} \; + \; \oint\limits_{C(t)} \mathbf{V} \cdot d\mathbf{V} \tag{2.49}$$

The second closed integral on the right side vanishes since $\mathbf{V} \cdot d\mathbf{V} = d\left(\frac{1}{2}\mathbf{V} \cdot \mathbf{V}\right)$ is the total differential of a single-valued function, and the starting point of integration coincides with the end point.

Using Euler's equation, which is given by Equation (2.1) with $\nu = 0$, we have

$$\begin{aligned} \frac{D\mathbf{V}}{Dt} &= \frac{\partial \mathbf{V}}{\partial t} + (\mathbf{V} \cdot \boldsymbol{\nabla}) \; \mathbf{V} \\ &= -\frac{1}{\rho}\boldsymbol{\nabla} p + \mathbf{F} \end{aligned}$$

Equation (2.49) can be rewritten as

$$\frac{D\Gamma}{Dt} = \oint\limits_{C(t)} \left(-\frac{1}{\rho}\boldsymbol{\nabla} p + \mathbf{F}\right) \cdot d\mathbf{R}$$

and we conclude from this that $D\Gamma/Dt$ vanishes if $\left(-\dfrac{1}{\rho}\boldsymbol{\nabla} p + \mathbf{F}\right)$ can be written as a total differential. If the body forces per unit mass are irrotational (i.e., $\boldsymbol{\nabla} \times \mathbf{F} = \mathbf{0}$), a potential function F exists such that

$$\mathbf{F} = -\boldsymbol{\nabla} F$$

and hence for an homogeneous density field, or more generally for a barotropic flow,

$$\begin{aligned} \left(-\frac{1}{\rho}\boldsymbol{\nabla} p + \mathbf{F}\right) \cdot d\mathbf{R} &= -\left(\frac{1}{\rho}\boldsymbol{\nabla} p + \boldsymbol{\nabla} F\right) \cdot d\mathbf{R} \\ &= -\boldsymbol{\nabla}\left(\frac{1}{\rho} p + F\right) \cdot d\mathbf{R} \\ &= -\boldsymbol{\nabla} P \cdot d\mathbf{R} \\ &= -dP \end{aligned}$$

where $P = \left(\dfrac{p}{\rho} + F\right)$ and the first integral on the right side also vanishes. This result is known

as *Thompson's vortex theorem* or *Kelvin's circulation theorem*:

$$\frac{D\Gamma}{Dt} = 0 \tag{2.50}$$

In words: *In an inviscid, barotropic fluid, the circulation around a closed material line remains constant for all times if the body forces per unit mass have a potential.*

According to Stoke's theorem, the line integral $\oint\limits_{C(t)} \mathbf{V} \cdot d\mathbf{R}$ around the closed curve C is equal to the surface integral $\iint\limits_{S(t)} (\boldsymbol{\nabla} \times \mathbf{V}) \cdot \mathbf{n}\, dS$ over any surface of arbitrary shape which has C as its boundary; therefore Equation (2.48) can also be rewritten as:

$$\Gamma = \oint\limits_{C(t)} \mathbf{V} \cdot d\mathbf{R} = \iint\limits_{S(t)} \boldsymbol{\Omega} \cdot \mathbf{n}\, dS \tag{2.51}$$

Vortex lines are the vorticity field lines. In complete analogy to streamtubes, we can use them to form vortex tubes (Figure 2-7). Next, we show that at any instant the circulation around a vortex tube is constant along its length and discuss the ramifications.

The vortex lines that pass through a closed curve C form a vortex tube. According to Stoke's theorem, the line integral over the closed curve in Figure 2-8 vanishes, because the integrand in the second integral on the right-hand side of Equation (2.51) is zero, since $\boldsymbol{\Omega} = \boldsymbol{\nabla} \times \mathbf{V}$ is by definition perpendicular to $\mathbf{n}$. The contributions to the integral from the infinitely close pieces C_3 and C_4 of the curve cancel each other and we are led to the equation

$$\int\limits_{C_1(t)} \mathbf{V} \cdot d\mathbf{R} + \int\limits_{C_2(t)} \mathbf{V} \cdot d\mathbf{R} = 0 \tag{2.52}$$

Because of the infinitesimally small distance between the curves C_3 and C_4, we can consider C_1 and C_2 to be closed curves. If we change the direction of integration over C_2, thereby changing the sign of the second integral, we obtain *Helmholtz's first vortex theorem*:

$$\oint\limits_{C_1(t)} \mathbf{V} \cdot d\mathbf{R} = \oint\limits_{C_2(t)} \mathbf{V} \cdot d\mathbf{R} \tag{2.53}$$

In words: *At any instant, the circulation around a vortex tube is constant along its length.* From this derivation the kinematic nature of this theorem is obvious.

Another approach to this important theorem starts from considering the fact that the vorticity is a divergenceless field, i.e. $\boldsymbol{\nabla} \cdot \boldsymbol{\Omega} = \boldsymbol{\nabla} \cdot (\boldsymbol{\nabla} \times \mathbf{V}) = 0$. We can consider the vorticity field $\boldsymbol{\Omega}(\mathbf{R}, t)$ as the velocity field of a new incompressible flow, i.e. the vortex tube becomes the streamtube of the new field. We apply the equation of continuity for an incompressible flow in its integral form

$$\iint_{S(t)} \mathbf{V} \cdot \mathbf{n} \, dS = 0$$

to a part of this streamtube, and at the same time we replace $\mathbf{V}$ by $\boldsymbol{\Omega}$. Since the new "flow" is also incompressible, we obtain

$$\iint_{S(t)} \boldsymbol{\Omega} \cdot \mathbf{n} \, dS = 0 \tag{2.54}$$

i.e., for every closed surface S, the flux of the vorticity is zero. We now apply Equation (2.54) to a part of the vortex tube whose closed surface consists of the surface of the vortex tube and two arbitrarily orientated cross-sections A_1 and A_2 (see Figure 2-9), and find

$$\iint_{A_1(t)} \boldsymbol{\Omega} \cdot \mathbf{n} \, dS + \iint_{A_2(t)} \boldsymbol{\Omega} \cdot \mathbf{n} \, dS = 0 \tag{2.55}$$

since the integral over the vortex tube surface vanishes. The integral $\iint \boldsymbol{\Omega} \cdot \mathbf{n} \, dS$ is often called the *vortex strength*. It is clearly identical to the circulation, and in words Equation (2.55) reads: *At any instant, the strength of a vortex tube is constant along its length.* Noting the sense of integration of the line integral, we can use Stoke's theorem to transform Equation (2.55) into Helmholtz's first theorem (2.53). We conclude from this representation that, just like the streamtube, the vortex tube cannot begin or end within the fluid. A tube must extend to infinity, or end at the boundaries of the fluid, or form a ring.

We now consider *Helmholtz's second vortex theorem*: *A vortex tube always consists of the same fluid particles.* A vortex tube is therefore a material tube. To obtain this theorem as a direct consequence of Kelvin's circulation theorem we consider a vortex tube and an arbitrary closed curve on its surface at time t_0 (see Figure 2-10). By Stoke's integral theorem, the

circulation around the closed curve is zero. The circulation of the curve, which is made up of the same material particles, still has the same value of zero at a later instant of time t, since by Kelvin's circulation theorem $D\Gamma/Dt = 0$. By inverting the above reasoning, we conclude that it follows from Stoke's theorem that these material particles must be on the outer surface of a vortex tube.

Finally we consider *Helmholtz's third vortex theorem*, which reads: *The circulation around a vortex tube remains constant in time.* This follows immediately from Helmholtz's second theorem together with Kelvin's circulation theorem: a closed line generating the vortex tube is, by Helmholtz's second theorem, a material line whose circulation, by Kelvin's theorem, remains constant.

It is important to emphasize that the Kelvin-Helmholtz theorems apply only in the region where shear stresses (viscous effects) are ignorable and the relationship between pressure and density is single-valued. In this work the density is assumed to be constant while the pressure is continuous everywhere except across the lifting surfaces. Therefore, in order to render the wake force-free the Kelvin-Helmholtz theorems require that all the vorticity must be transported with the fluid particles and vortex filaments in the wake must always be composed of the same fluid particles. The discontinuity in pressure across the lifting surfaces gives the aerodynamic forces and moments.

2.9 The Unsteady Vortex-Lattice Method

2.9.1 Introduction

In the present study, a general unsteady vortex-lattice method is used to obtain the aerodynamic loads. This is an extension of the well known vortex-lattice method that has been used with considerable success to treat steady flows at subsonic velocities. The present method can be applied to either two-dimensional or three-dimensional lifting and nonlifting flows. It is not limited by planform, camber, twist, or angle of attack. The surface of the body may undergo any time-dependent deformation, and the body can execute any maneuver in moving air. A body may be viewed as moving through air either at rest or in motion; thus, the effect of gusts on a maneuver can also be modeled. The only restrictions are that separation occurs along the

sharp edges and vortex bursting does not occur near the surface. The flow surrounding the body (here either an aircraft or a bridge) is assumed to be irrotational, and incompressible over the entire flowfield, except next to the solid boundaries of the body and in the wakes.

The solutions are evaluated in the time domain and they are not restricted to small periodic motions. This approach allows nonlinear and unsteady aerodynamic effects to be included in the aeroelastic model. Thus, the effects of static deformations and large angles of attack may be incorporated into the model of the system. The vortex-lattice method can accommodate more than one body; thus, steady and unsteady aerodynamic interference can be modeled with accurate estimates of the phasing among loads.

The method treats the position of, and the distribution of vorticity in, the wakes as unknown. It accounts for leading-edge separation on highly swept delta and delta-like wings, and for wing-tip vortex systems on low-aspect rectangular, swept, and tapered wings. In all calculations the recent history of the flow is taken into account. The present method employs an explicit routine for generating the unsteady wake (instead of the iterative scheme that was used previously by some investigators), providing efficiency without a loss of accuracy and even providing solution for some cases where the iterative methods did not converge.

2.9.2 Coordinate Systems for the Aircraft

Three coordinate frames, a ground-fixed or Newtonian frame (N), a moving or body-fixed frame (B), and an elastic-axis frame (E) are used. The body-fixed and elastic-axis frames are attached to the airplane and follow it through all of its maneuvers. Since the wing is deforming, the elastic-axis frame is attached to some reference point on the fuselage. The problem is posed in terms of the body-fixed and the elastic-axis frames. The motion of the wing and the motion of the ambient fluid may be specified as arbitrary functions of time.

The three coordinate systems are shown in Figure 2-11. The base vectors for the N-frame (X_1, X_2, X_3) are denoted by $(\hat{\mathbf{n}}_1, \hat{\mathbf{n}}_2, \hat{\mathbf{n}}_3)$, those for the B-frame (x_1, x_2, x_3) by $(\hat{\mathbf{b}}_1, \hat{\mathbf{b}}_2, \hat{\mathbf{b}}_3)$, and those for the E-frame (ξ, η, ζ) by $(\hat{\mathbf{e}}_1, \hat{\mathbf{e}}_2, \hat{\mathbf{e}}_3)$.

These three coordinate frames are used to transfer information between the programs NASTRAN and CATIA. NASTRAN is used to model the structure of the wing and CATIA is used to define the geometry of the complete aircraft. The N-frame is first introduced in CATIA to

define points on the surface of the aircraft, and the X_1, X_2, and X_3 axes are commonly called Fuselage-Station (F.S.), Butt-Line (B.L.), and Water-Line (W.L.) respectively. NASTRAN uses this system as the basic (also called 0) reference frame. However this frame is not convenient for the structural analysis of the wing. To describe (view) elastic deformations and to use in the analysis of flight dynamics, we introduce the B-frame. This system usually has its origin close to the mass center of the complete aircraft. For the structural analysis of components local coordinate systems are introduced; the E-frame is such a system. NASTRAN provides several options to automatically generate the B and E systems from the N-frame. For the problem considered later, the structural model for the wing is a beam, and the y-axis lies along the undeformed elastic axis.

The position vectors can be written in terms of their components in the N and B coordinate systems as follows:

$$\mathbf{R} = X_1\ \hat{\mathbf{n}}_1 + X_2\ \hat{\mathbf{n}}_2 + X_3\ \hat{\mathbf{n}}_3 \tag{2.56}$$

$$\mathbf{r} = x_1\ \hat{\mathbf{b}}_1 + x_2\ \hat{\mathbf{b}}_2 + x_3\ \hat{\mathbf{b}}_3 \tag{2.57}$$

It follows from Figure 2-11 that the position of a point in the N-frame can be expressed

$$\mathbf{R} = \mathbf{R}_B + \mathbf{r} \tag{2.58}$$

where $\mathbf{R}_B$ is the position of the origin of the B-frame with respect to the N-frame.

Taking the substantial derivative of Equation (2.58) we obtain the velocity of any fluid particle with respect to the N frame; that is,

$$\mathbf{V} = \mathbf{V}_B + {}^N\boldsymbol{\omega}^B \times \mathbf{r} + \mathbf{v} \tag{2.59}$$

where $\mathbf{V}_B = \dfrac{{}^N d\mathbf{R}_B}{dt}$ is the absolute velocity (i.e., velocity with respect to the N-frame) of the origin of the B-frame, ${}^N\boldsymbol{\omega}^B$ is the angular velocity of the B-frame with respect to the N-frame, and $\mathbf{v} = \dfrac{{}^B d\mathbf{r}}{dt}$ is the velocity of the fluid particle relative to the B-frame. The components of the angular velocity in the B-frame can be expressed in terms of the Euler angles and their derivatives.

2.9.3 Coordinate Systems for Bridges

For the aeroelastic analysis of long-span bridges we use a system fixed to the ground (N), one fixed to the roadbed (B), and one fixed to each wing (W_i) (see Figure 2-12). The use of coordinate systems attached to the moving parts facilitates describing the aerodynamic grids, imposing the zero normal flow boundary condition on the surface of the body, and deriving the equations of motion.

2.9.4 The Mathematical Problem

In this work, we develop an aerodynamic model that can be used to simulate a body or bodies moving through moving air. As a result of the relative motion between the body and the fluid, vorticity is generated in a thin region adjoining the surface of the body (the boundary layer). Wherever two streams with different energy merge, such as along the trailing edge of the wing, at the exit of the engine, etc., we require the pressures in the two streams to be the same. In general, this requirement can be satisfied only when vorticity is shed from the body. This shed vorticity convects away from the body and forms the wakes. In the model we restrict all the vorticity in the flow to a thin region around the boundaries of the body and its wakes and consider the flow outside this region to be irrotational. We consider the boundary layers and the wakes to be sheets of vorticity. There are two types of vortex sheets (see Figure 2-13): the bound-vortex sheet, and the free-vortex sheet.

The bound-vortex sheet represents the boundary layer on the surface of the body. These infinitesimally thin layers of vorticity may be viewed as the infinite-Reynolds-number approximation to the actual boundary layers. Therefore, one can expect the present model to improve as the Reynolds number increases. For the case of thin wings, the vortex sheets on the upper and lower surfaces are merged into a single surface composed of the camber lines. The position of the bound-vortex sheet is specified (i.e. it does not move with the fluid particles); as a result a finite pressure jump exists across it in general.

The free-vortex sheets represent the wakes. Their positions are not specified a priori; they are allowed to deform freely during the solution until they assume force-free positions. The two types of vortex sheets are joined along the sharp edges where separation occurs, the same edges where the Kutta condition is imposed in a steady flow.

The problem under consideration here is that of high-Reynolds-number flow of an incompressible fluid. We let $\mathbf{V}(\mathbf{R},t)$ denote the absolute velocity of a fluid particle at any point $\mathbf{R}$ of the flowfield at time t, $p(\mathbf{R},t)$ the fluid pressure at that point, and ρ the constant fluid density. If the Reynolds number is very large and the density is taken as constant, the general Navier-Stokes equations, (2.1), reduce to the well-known Eulerian equation of motion outside the boundary layers and wakes

$$\frac{\partial \mathbf{V}}{\partial t} + (\mathbf{V} \cdot \boldsymbol{\nabla}_{\mathbf{R}})\ \mathbf{V} = -\frac{1}{\rho}\boldsymbol{\nabla}_{\mathbf{R}}\ p \tag{2.60}$$

and the continuity Equation (2.2) is given by

$$\boldsymbol{\nabla}_{\mathbf{R}} \cdot \mathbf{V} = 0$$

In Equation (2.60) all body forces, such as gravity, have been assumed to be conservative, and their potentials have been absorbed in the pressure. Equations (2.60) and (2.2) are valid in the outer field of flow, that is, the region exterior to the boundary surfaces, boundary layers, and wakes.

To these equations must be added certain boundary conditions. We assume that the locations of the boundary surfaces are known, possibly as functions of time, and the normal component of the fluid velocity is prescribed on this boundaries. In general there will be several bodies moving relative to each other. The entire boundary will be denoted by S. The first boundary condition requires the normal component of the velocity of the fluid relative to the body to be zero at the boundaries of the body. This boundary condition, commonly called the no-penetration boundary condition, becomes:

$$(\mathbf{V} - \mathbf{V}_S) \cdot \mathbf{n} = 0 \text{ on } S \tag{2.61}$$

where $\mathbf{V}_S$ is the velocity of the boundary surface S, and $\mathbf{n}$ is the unit normal vector. In general, $\mathbf{V}_S$ and $\mathbf{n}$ vary in space and time. In order to model nonzero velocities across the boundaries,

a transpiration velocity $\mathbf{V}_N$ is added, so engine inlet/exit flows can be modeled:

$$(\mathbf{V} - \mathbf{V}_S) \cdot \mathbf{n} = \mathbf{V}_N \cdot \mathbf{n} \tag{2.62}$$

For the exterior problem a regularity condition at infinity must also be imposed. It is important to emphasize, that the above equations do not define a potential flow, which is a consequence of the condition of irrotationality. The usual way to derive the equations of potential flow is by assuming that the velocity field $\mathbf{V}(\mathbf{R}, t)$ is irrotational and that it can therefore be expressed as the gradient of a potential function. This is true for flows that can be generated from rest by the action of conservative body forces or by motion of the boundaries. In this thesis, a slightly more general class of flows is considered. The velocity field $\mathbf{V}(\mathbf{R}, t)$ is expressed as the sum of two velocities:

$$\mathbf{V} = \mathbf{V}_\infty + \mathbf{U} \tag{2.63}$$

The vector $\mathbf{V}_\infty$ is the velocity of the onset flow, which is defined as the velocity field that would exist in the fluid if all the boundaries disappeared. The vector field $\mathbf{U}(\mathbf{R}, t)$ is the disturbance velocity field created by the body. The velocity field $\mathbf{U}(\mathbf{R}, t)$ is associated with the vorticity in the sheets that simulate the wakes and the boundary layers on the surface of the body. Anywhere off these sheets, $\mathbf{U}(\mathbf{R}, t)$ is irrotational, and hence, may be expressed as the gradient of a potential function $\Psi(\mathbf{R}, t)$,

$$\mathbf{U}(\mathbf{R}, t) = \boldsymbol{\nabla}_{\mathbf{R}} \Psi(\mathbf{R}, t) \tag{2.64}$$

Since $\mathbf{V}_\infty$ is the velocity of an incompressible flow, it satisfies Equation (2.2), i.e. $\boldsymbol{\nabla}_{\mathbf{R}} \cdot \mathbf{V}_\infty = 0$, and thus $\mathbf{U}(\mathbf{R}, t)$ does too; that is,

$$\boldsymbol{\nabla}_{\mathbf{R}} \cdot \mathbf{U} = 0 \tag{2.65}$$

Using $\mathbf{U}(\mathbf{R}, t)$ from Equation (2.64) in Equation (2.65) gives the expected result: the potential $\Psi(\mathbf{R}, t)$ satisfies Laplace's equation,

$$\boldsymbol{\nabla}^2_{\mathbf{R}} \Psi(\mathbf{R}, t) = 0 \tag{2.66}$$

in the region occupied by the fluid. The boundary conditions on $\Psi(\mathbf{R}, t)$ arise from (2.61), (2.62), (2.63), and (2.64) in the form

$$\boldsymbol{\nabla}_{\mathbf{R}}\Psi \cdot \mathbf{n}|_S = \left.\frac{\partial \Psi}{\partial \mathbf{n}}\right|_S = (-\mathbf{V}_\infty + \mathbf{V}_S) \cdot \mathbf{n}|_S \tag{2.67}$$

and

$$\boldsymbol{\nabla}_{\mathbf{R}}\Psi \cdot \mathbf{n}|_S = \left.\frac{\partial \Psi}{\partial \mathbf{n}}\right|_S = (-\mathbf{V}_\infty + \mathbf{V}_S + \mathbf{V}_N) \cdot \mathbf{n}|_S \tag{2.68}$$

In the exterior problem, the second boundary condition requires that the flow disturbance, due to the motion of the body (or bodies) through the fluid, should diminish far from the body. This is usually called the regularity condition at infinity and is given by

$$\lim_{\|\mathbf{R}-\mathbf{R}_B\|_2 \to \infty} \|\boldsymbol{\nabla}_{\mathbf{R}}\Psi\|_2 = 0 \tag{2.69}$$

The disturbance velocity field is computed according to the Biot-Savart law; thus, this equation and, hence, the regularity condition at infinity are satisfied identically. At this point a few facts must be emphasized. From the previous results we can see that for incompressible potential flow the velocity field is determined by the equation of continuity (2.66). Thus the equation of motion (2.60) is not used, and the velocity may be determined independent of the pressure. Once the velocity field is known, the pressure is calculated from the equation of motion (2.60), which can be integrated to produce the Bernoulli equation. Moreover, since the speed of sound is assumed to be infinite, the influence of the boundary conditions is immediately radiated across the whole fluid region; therefore, the instantaneous velocity field is obtained from the instantaneous boundary conditions.

In addition to the boundary conditions, the Kelvin-Helmholtz theorems and the unsteady Kutta condition are used to determine the strength and position of the free-vortex sheets (the wakes).

2.9.5 Discretization of the Vortex Sheets

In the unsteady vortex-lattice method, we replace the bound-vortex sheet by a lattice of short, straight vortex segments of constant circulation $\Gamma_i(t)$. These segments divide the surface of the

body into a number of elements of area. This is shown in Figure 2-14. The model is completed by joining free vortex lines, representing the continuous free-vortex sheets, to the bound-vortex lattice along the edges of separation; such as the trailing edges of lifting surfaces, exits of the engines, etc., as shown in Figure 2-15.

Experience with the vortex-lattice method suggests that the geometric shape of the elements in the lattice affects the accuracy and the rate of convergence. It was found that rectangular elements work better than other shapes. Consequently, as much as possible we use rectangular, or nearly rectangular, elements everywhere except in those places where we are forced to use triangular elements: for example, at the nose of the aircraft, the inlet of the engine, etc.

Each element of area in the lattice is enclosed by a loop of vortex segments; a portion of the lattice is represented in Figure 2-16. The unknowns are the circulations around the individual segments; the equations are the no-penetration condition for each element and the statement of conservation of circulation. In Figure 2-16 for example, there are 58 unknowns. Instead of solving for 58 unknowns from 58 equations, we can substantially reduce the size of the problem and obtain the solution in less time. The latter is an important consideration for unsteady flows where the solution must be recomputed at each time step.

To reduce the size of the problem, we can consider each element to be enclosed by a closed loop of vortex segments having the same circulation. Then the requirement of spatial conservation of circulation is automatically satisfied. These loop circulations are denoted by $G_i(t)$, in Figure 2-17 (where $i = 1, \ldots, 24$; hence, the problem is reduced to one of finding 24 unknowns instead of 58). But now each of the straight segments (except possibly those in the leading row of the lifting surfaces) is formed from parts of two loops. For example the circulation around the segment that connects nodes 8 and 13 in Figure 2-16, which is denoted by $\Gamma_{16}(t)$, is given by $G_7(t) - G_6(t)$. In order to distinguish nodes on the lattice, such as nodes 8 and 13, from nodes in the discretized structural model (discussed in the next chapter), we call them *aerodynamic nodes*.

Because we approximated the vortex sheets with a lattice, we can satisfy the no-penetration condition given by Equations (2.67) or (2.68) at only a finite number of points, the so called control points of the bound lattice. The control points are the centroids of the corner points (aerodynamic nodes), and the unit normal vector of each element is obtained from the cross

product of the two diagonals. For a four-sided element, the control point and the unit normal vector are represented in Figure 2-18. Triangular elements are handled by having two corners coincide.

The problem consists of finding the circulations $G_i(t)$ around the closed loops of discrete vorticity such that the velocity field $\mathbf{V} = \mathbf{V}_\infty + \mathbf{U}$ satisfies conditions (2.67) or (2.68) at the control points. Here, we explain the computational procedure by means of an example.

2.9.6 Impulsive Start

We consider a wing that impulsively starts to move with constant velocity through a fluid that would otherwise be at rest, i.e. $\mathbf{V}_\infty = \mathbf{0}$. A lattice of 4×6 elements simulates half of the wing and the flow is symmetric; Figure 2-19 shows half of the lattice. Before the motion begins, we set all the circulations equal to zero. At $t = 0$ the motion begins and the circulations in the bound portion of the lattice change instantaneously. A discrete vortex line is formed along the sharp edges; it represents the starting vortex observed in experiments and described by Prandtl [179]. Here the existence of the starting vortex is dictated by the requirement of spatial conservation of circulation discussed before.

In order to satisfy the Kutta condition, the vortex segments along the trailing edge and tip of the wing are convected into the wake at the local particle velocity. At the instant that the motion begins, no vorticity has been convected; thus, there is no wake.

In order to find the circulations, we construct a matrix of influence coefficients $A_{ij}(t)$ for $i, j = 1, 2, \ldots, N$ where N is the number of elements (closed loops of constant vorticity) in the bound lattice. The coefficient $A_{ij}(t)$ represents the normal component of the velocity at the control point of the i-th element associated with a closed loop of vorticity around the j-th element having unit circulation, and is in general a function of time (see Figure 2-20). In Figure 2-20, the j-th element is called the sending element and appears as the shaded element; the i-th element is called the receiveing element and appears without shading. Element i is receiving the disturbance sent by element j.

Multiplying $A_{ij}(0)$ by the actual circulation for the j-th element, $G_j(0)$, and then summing for all j, we obtain the normal component of the velocity at the control point of the i-th element associated with all the bound vortices. Therefore, the no-penetration condition given

by Equation (2.67) can be written as follows:

$$\sum_{j=1}^{N} A_{ij}\,(0)\;\; G_j\,(0) = \mathbf{V}_S\,(\mathbf{r}_i, 0)\cdot \mathbf{n}\,(\mathbf{r}_i, 0) \quad \text{for} \quad i = 1, 2, \ldots, N \tag{2.70}$$

where $\mathbf{r}_i$ is position vector in the B-frame of the control point of the i-th element, $\mathbf{n}\,(\mathbf{r}_i, 0)$ is the unit normal vector at that control point at time $t = 0$, and $\mathbf{V}_\infty$ has been set equal to zero. As we explicitly indicate in Equation (2.70), the velocity of the surface of the wing, the circulations, the unit normal vectors, the relative positions of the aerodynamic nodes, and hence the influence coefficients are functions of time. In the particular case in which the body is rigid (i.e. the relative positions of the aerodynamic nodes do not change), the A_{ij} and $\mathbf{n}\,(\mathbf{r}_i, t)$ remain constant. However, in general, the body does deform and the influence coefficients $A_{ij}\,(t)$, the unit normal vectors $\mathbf{n}\,(\mathbf{r}_i, t)$, etc., must be computed at each time step.

The linear algebraic system of equations given by Equation (2.70) can be solved for the unknown circulations $G_j\,(0)$ by using either a direct procedure, such as LU decomposition or Gauss elimination, or an iterative procedure, such as the Jacobi or the Gauss-Seidel method. According to Konstadinopoulos et al. [180], since the values of the circulations corresponding to two consecutive time steps are very close, the solution is amenable to an iterative procedure.

To begin the solution at the next time step, $t = \Delta t$, we convect the starting vortex at the local particle velocity. The local velocity relative to the moving frame is computed at each aerodynamic node of the discrete vortex line along the trailing edge and wing-tip from Equation (2.59)

$$\mathbf{v} = \mathbf{V} - \mathbf{V}_B - \;{}^{N}\boldsymbol{\omega}^{B} \times \mathbf{r} \tag{2.71}$$

where $\mathbf{V}$ is the absolute velocity of the fluid particle, calculated from the Biot-Savart law, and $\mathbf{v}$ is the velocity of the fluid particle relative to the B-frame.

We use Equation (2.71) to determine the displacements, $\Delta\mathbf{r}$, of the aerodynamic nodes in the B-frame:

$$\Delta\mathbf{r} = \int_0^{\Delta t} \mathbf{v}\; dt \tag{2.72}$$

We approximate the value of $\Delta\mathbf{r}$. Because all these quantities are functions of time, the question of which instantaneous quantities to use in the approximation is raised. There are

several options: for example, one can use the quantities that were calculated at the previous time step ($t = 0$), the quantities at the present time step ($t = \Delta t$), or their averaged values for the two time steps. In all cases except the first, iterations are needed, which increase the computational time. Kandil et al. [77] showed that the first option is stable and there are little differences in the computed results for the various options; therefore, the first option was used to compute all the results in this thesis.

In Figure 2-21 the segment of the starting vortex at the trailing edge connecting nodes 10 and 15 is represented by an arrow from point P_{10} to point P_{15}, with a circulation $\Gamma_{18}(0)$. At the next time step, Figure 2-22, this segment of the starting vortex is convected to the new position denoted by P_{37} and P_{38}. The circulation is still $\Gamma_{18}(0)$ in order to satisfy the temporal conservation of circulation. Simultaneously, a new starting vortex is formed between P_{10} and P_{15} in Figure 2-22 with circulation $\Gamma_{18}(\Delta t)$. In order to satisfy spatial conservation of circulation, we must join the two starting vortices at the nodal points with the connectors shown in Figure 2-22. The length and direction of the connectors are computed from the approximated version of Equation (2.72) as follows:

$$(P_{10}P_{37}) = \mathbf{r}_{37} - \mathbf{r}_{10} = \mathbf{v}(\mathbf{r}_{10}, 0)\ \Delta t \tag{2.73}$$

$$(P_{15}P_{38}) = \mathbf{r}_{38} - \mathbf{r}_{15} = \mathbf{v}(\mathbf{r}_{15}, 0)\ \Delta t \tag{2.74}$$

Now we calculate the bound circulations for the time $t = \Delta t$. Equations (2.70) are no longer valid because they do not take into account the existence of the wake. Hence, the no-penetration condition given by Equation (2.67) must be modified as follows:

$$\sum_{j=1}^{N} A_{ij}(\Delta t)\ G_j(\Delta t) = [\mathbf{V}_S(\mathbf{r}_i, \Delta t) - \mathbf{V}_W(\mathbf{r}_i, \Delta t)] \cdot \mathbf{n}(\mathbf{r}_i, \Delta t) \quad \text{for} \quad i = 1, 2, \ldots, N \tag{2.75}$$

where $\mathbf{V}_W(\mathbf{r}, \Delta t)$ is the velocity field, at time $t = \Delta t$, associated with the vorticity in the wake, whose position and circulation are already known. After we calculate $G_j(\Delta t)$ from Equations (2.75),we proceed to the next time step, $t = 2\Delta t$.

In Figure 2-23, the wake is represented after two time steps. The same figure includes the new positions of the two previously shed vortices and the newly formed starting vortex. There

is vorticity along the lines from P_{10} to P_{37} (P_{15} to P_{38}) and from P_{37} to P_{47} (P_{38} to P_{48}). During the second time step, all the vorticity that lay along the line from P_{10} to P_{37} (P_{15} to P_{38}) was convected and now lies along the line from P_{37} to P_{47} (P_{15} to P_{38}). In the present model, all the starting vorticity generated at each time step is shed and convected. Referring to Figure 2-23 again, we see that this is accomplished by simply convecting the entire closed loop of vorticity from the elements along the sharp edges of the bound lattice into the wake.

Because the vorticity varies along the edges (e.g., $G_8(t) \neq G_4(t)$ and $G_{12}(t) \neq G_8(t)$ for $t = 0,\ \Delta t,\ 2\Delta t, \ldots$) *the vorticity along the connectors is not zero.* For example in Figure 2-23, the circulation around the line from P_{10} to P_{37} is $G_4(\Delta t) - G_8(\Delta t)$, while the circulation around the line from P_{37} to P_{47} is $G_4(0) - G_8(0)$.

The procedure described above can be continued for any desired number of steps. At each new time step, a new starting vortex is formed, shed, and convected away from the edge to form the wake. The vorticity in the near wake can significantly affect the flowfield next to the body, the distribution of vorticity on its surface and, hence, the loads on the body. Because the vorticity in the wake now was generated on, and shed from, the body at an earlier time, the flowfield is history-dependent and so the current distribution of vorticity on the surface of the body depends to some extent on the previous distributions of vorticity. The vorticity distribution in and the shape of the wake are determined as part of the solution so the history of the motion is stored in the wake. We say that the wake is the "historian" of the flow. As time passes and the vorticity in the wake convects far downstream, its associated velocity field does not have any appreciable influence on the flow around the body; thus, the historian has a fading memory. In the numerical method, this means that only the wake near to the body is important; the rest can be safely neglected.

In Figures 2-24 and 2-25 we present an actual solution showing how the wake develops for the wing of the aircraft used in one of the numerical examples in this thesis after an impulsive start. The solutions after 5, 10, 15, 25, and 50 time steps, as well as the steady-state solution ($t \to \infty$) are given. The flow in Figures 2-24 and 2-25 is symmetric, but symmetry is not a requirement. This example considered an impulsively started wing, but the method can accommodate any complete description (circulations and positions) of the wake as an initial condition.

The flow associated with the vorticity can significantly affect the wing. In Figure 2-26 there

is a photograph of the wake behind a crop duster. It is visible because of the herbicide in the swirling flow. Clearly, the region affected by the vorticity in the wing-tip vortex is quite large, but the vorticity is concentrated in a fair small region near the center of the clear space. This center region is clear because it contains air that entered this flow through the core of the wing-tip vortex along the wing tip and did not mix with the herbicide being emitted along a line near the trailing edge.

2.10 Dimensionless Variables

It is desirable to have uniform elements in the lattice. In order to achieve this objective, the models are nondimensionalized by using the following characteristic variables of length, velocity and density:

L_C is the chordwise length of one element on the bound lattice,

V_C is either the undisturbed freestream velocity of the fluid or a speed characterizing the forward motion of the body,

ρ_C is the freestream density of the fluid.

From these definitions the characteristic time T_C can be defined as $T_C = \dfrac{L_C}{V_C}$. The choices for L_C and V_C are convenient for two reasons. First, an increase in the number of elements in the chordwise direction of the bound lattice automatically leads to a corresponding decrease in the physical time step. Second, a dimensionless time step of value one (i.e., $\Delta t = T_C$) creates wake elements of approximately the same dimensions as the elements on the lifting surfaces.

2.11 Unsteady Bernoulli Equation

The computation of the aerodynamic load on each area element of the bound lattice is performed by determining the pressure jump across its surface and then multiplying it by the area of the element. These pressure jumps are found from Bernoulli's equation for unsteady flows:

$$\left.\frac{\partial \Phi^*\left(\mathbf{R}^*, t^*\right)}{\partial t^*}\right|_{\mathbf{R}^*} + \frac{1}{2}\nabla_{\mathbf{R}^*}\Phi^*\left(\mathbf{R}^*, t^*\right) \cdot \nabla_{\mathbf{R}^*}\Phi^*\left(\mathbf{R}^*, t^*\right) + \frac{p^*\left(\mathbf{R}^*, t^*\right)}{\rho^*} = H^*\left(t^*\right) \tag{2.76}$$

Here, asterisks denote dimensional quantities. The total velocity potential is indicated by

$\Phi^*(\mathbf{R}^*, t^*)$, i.e.,

$$\nabla_{\mathbf{R}^*}\Phi^*(\mathbf{R}^*, t^*) = \mathbf{U}^*(\mathbf{R}^*, t^*) + \mathbf{V}^*_\infty \tag{2.77}$$

$$= \mathbf{V}^*(\mathbf{R}^*, t^*) \tag{2.78}$$

and $\mathbf{V}^*(\mathbf{R}^*, t^*)$ is the absolute velocity, $p^*(\mathbf{R}^*, t^*)$ is the unknown pressure, ρ^* is the constant density of the fluid, and $H^*(t^*)$ is a spatially uniform function of time. At large distances from the body and its wakes, i.e. as $\|\mathbf{R}^*\|_2 \to \infty$, $\Phi^* \to \Phi^*_\infty =$ constant in time, $p^* \to p^*_\infty =$ constant, and $\nabla_{\mathbf{R}^*}\Phi^* \to \mathbf{V}^*_\infty$, the velocity of the freestream. Hence we let $H^*(t^*) \to \frac{1}{2}\mathbf{V}^*_\infty \cdot \mathbf{V}^*_\infty + \frac{p^*_\infty}{\rho^*}$, a constant, and write Equation (2.76) as

$$\left.\frac{\partial \Phi^*}{\partial t^*}\right|_{\mathbf{R}^*} + \frac{1}{2}\mathbf{V}^* \cdot \mathbf{V}^* + \frac{p^*}{\rho^*} = \frac{1}{2}\mathbf{V}^*_\infty \cdot \mathbf{V}^*_\infty + \frac{p^*_\infty}{\rho^*} \tag{2.79}$$

or

$$\frac{p^*}{\rho^*} - \frac{p^*_\infty}{\rho^*} = \frac{1}{2}\mathbf{V}^*_\infty \cdot \mathbf{V}^*_\infty - \frac{1}{2}\mathbf{V}^* \cdot \mathbf{V}^* - \left.\frac{\partial \Phi^*}{\partial t^*}\right|_{\mathbf{R}^*}$$

$$= \frac{1}{2}\mathbf{V}^*_\infty \cdot \mathbf{V}^*_\infty \left[1 - \frac{\mathbf{V}^* \cdot \mathbf{V}^*}{\mathbf{V}^*_\infty \cdot \mathbf{V}^*_\infty} - \frac{2}{\mathbf{V}^*_\infty \cdot \mathbf{V}^*_\infty}\left.\frac{\partial \Phi^*}{\partial t^*}\right|_{\mathbf{R}^*}\right] \tag{2.80}$$

but

$$\mathbf{V}^* \cdot \mathbf{V}^* = \|\mathbf{V}^*\|_2^2 = V^{*2}, \qquad \mathbf{V}^*_\infty \cdot \mathbf{V}^*_\infty = \|\mathbf{V}^*_\infty\|_2^2 = V^{*2}_\infty$$

then, Equation (2.80) can be rewritten as

$$\frac{p^*}{\rho^*} - \frac{p^*_\infty}{\rho^*} = \frac{1}{2}V^{*2}_\infty \left[1 - \left(\frac{V^*}{V^*_\infty}\right)^2 - \frac{2}{V^{*2}_\infty}\left.\frac{\partial \Phi^*}{\partial t^*}\right|_{\mathbf{R}^*}\right] \tag{2.81}$$

dividing both sides by $\frac{1}{2}V^{*2}_\infty$ we obtain

$$\frac{p^* - p^*_\infty}{\frac{1}{2}\rho^* V^{*2}_\infty} = 1 - \left(\frac{V^*}{V^*_\infty}\right)^2 - \frac{2}{V^{*2}_\infty}\left.\frac{\partial \Phi^*}{\partial t^*}\right|_{\mathbf{R}^*} \tag{2.82}$$

At this point we introduce the *pressure coefficient* C_p as

$$C_p = \frac{p^* - p_\infty^*}{\frac{1}{2}\rho^* V_\infty^{*2}} \tag{2.83}$$

And it follows from Equation (2.82) that

$$C_p = 1 - \left(\frac{V^*}{V_\infty^*}\right)^2 - \frac{2}{V_\infty^{*2}} \left.\frac{\partial \Phi^*}{\partial t^*}\right|_{\mathbf{R}^*} \tag{2.84}$$

It is convenient to introduce dimensionless variables

$$\mathbf{V}^*(\mathbf{R}^*, t^*) = V_C \ \mathbf{V}(\mathbf{R}, t), \quad \Phi^*(\mathbf{R}^*, t^*) = V_C L_C \ \Phi(\mathbf{R}, t) \tag{2.85}$$

$$\mathbf{R}^* = L_C \ \mathbf{R}, \quad t^* = T_C \ t \tag{2.86}$$

Now we can express $\dfrac{\partial \Phi^*}{\partial t^*}$ dimensionless by making use of the chain rule as follows

$$\begin{aligned} \frac{\partial \Phi^*}{\partial t^*} &= \frac{\partial \Phi^*}{\partial \Phi}\frac{\partial \Phi}{\partial t}\frac{\partial t}{\partial t^*} \\ &= \frac{V_C L_C}{T_C}\frac{\partial \Phi}{\partial t} \\ &= V_C^2 \frac{\partial \Phi}{\partial t} \end{aligned} \tag{2.87}$$

Therefore, using Equations (2.85), (2.86) and (2.87), one can rewrite Equation (2.84) in dimensionless form as

$$C_p = 1 - V^2 - 2 \left.\frac{\partial \Phi}{\partial t}\right|_{\mathbf{R}} \tag{2.88}$$

where $V = \|\mathbf{V}\|_2$. The pressure difference across the lifting surface at a point is defined as the pressure below the vortex sheet (point L) minus the pressure above the vortex sheet (point U), i.e.,

$$\Delta C_p = (C_p)_L - (C_p)_U \tag{2.89}$$

where

$$(C_p)_L = 1 - V_L^2 - 2 \left.\frac{\partial \Phi}{\partial t}\right|_{\mathbf{R}_L} \tag{2.90}$$

$$(C_p)_U = 1 - V_U^2 - 2\left.\frac{\partial \Phi}{\partial t}\right|_{\mathbf{R}_U} \tag{2.91}$$

Finally, introducing Equations (2.90) and (2.91) into (2.89), one finds

$$\begin{aligned} \Delta C_p &= V_U^2 - V_L^2 + 2\left(\left.\frac{\partial \Phi}{\partial t}\right|_{\mathbf{R}_U} - \left.\frac{\partial \Phi}{\partial t}\right|_{\mathbf{R}_L}\right) && (2.92) \\ &= \mathbf{V}_U \cdot \mathbf{V}_U - \mathbf{V}_L \cdot \mathbf{V}_L + 2\left(\left.\frac{\partial \Phi}{\partial t}\right|_{\mathbf{R}_U} - \left.\frac{\partial \Phi}{\partial t}\right|_{\mathbf{R}_L}\right) && (2.93) \end{aligned}$$

Next we consider the evaluation of $\mathbf{V}_U \cdot \mathbf{V}_U - \mathbf{V}_L \cdot \mathbf{V}_L$.

2.11.1 Evaluation of $\mathbf{V}_U \cdot \mathbf{V}_U - \mathbf{V}_L \cdot \mathbf{V}_L$

There is a jump in the tangential velocity across a vortex sheet equal to the strength of the sheet, or the circulation per unit length. The computed velocities relative to the lifting surface at the bound vortex sheet have no normal component because the no-penetration condition must be satisfied. The velocities on the upper and lower surfaces may be written as

$$\begin{aligned} \mathbf{V}_U &= \mathbf{V}_m + \frac{\Delta \mathbf{V}}{2} && (2.94) \\ \mathbf{V}_L &= \mathbf{V}_m - \frac{\Delta \mathbf{V}}{2} && (2.95) \end{aligned}$$

where $\Delta \mathbf{V}$ represents the jump in the tangential velocity across the vortex sheet and $\mathbf{V}_m$ is the "mean" velocity which does not recognize the presence of the local vorticity. It could be viewed as the velocity at the midpoint of the thickness of the vortex sheet. The difference $\mathbf{V}_U \cdot \mathbf{V}_U - \mathbf{V}_L \cdot \mathbf{V}_L$ can be rearranged as follows

$$\mathbf{V}_U \cdot \mathbf{V}_U - \mathbf{V}_L \cdot \mathbf{V}_L = (\mathbf{V}_U + \mathbf{V}_L) \cdot (\mathbf{V}_U - \mathbf{V}_L) \tag{2.96}$$

hence, using Equations (2.94) and (2.95) we can write

$$\mathbf{V}_U + \mathbf{V}_L = 2\mathbf{V}_m, \quad \mathbf{V}_U - \mathbf{V}_L = \Delta \mathbf{V} \tag{2.97}$$

and Equation (2.96) becomes

$$\mathbf{V}_U \cdot \mathbf{V}_U - \mathbf{V}_L \cdot \mathbf{V}_L = 2\mathbf{V}_m \cdot \Delta\mathbf{V} \tag{2.98}$$

Next we consider the evaluation of $\Delta\mathbf{V}$.

2.11.2 Evaluation of ΔV

We consider three cases individually: rectangular, parallelogram, and general elements.

Rectangular Element

A typical rectangular element is shown in Figure 2-27. The jump in the tangential velocity $\Delta\mathbf{V}$ across the element can be written as

$$\Delta\mathbf{V} = \Delta\mathbf{V}_1 + \Delta\mathbf{V}_2$$

where $\Delta\mathbf{V}_1$ and $\Delta\mathbf{V}_2$ are given by

$$\Delta\mathbf{V}_1 = -\frac{1}{\|\mathbf{L}_1\|_2}\left(\frac{\Gamma_2}{2} + \frac{\Gamma_3}{2}\right)\mathbf{e}_1 \tag{2.99}$$

$$\Delta\mathbf{V}_2 = \frac{1}{\|\mathbf{L}_3\|_2}\left(\frac{\Gamma_1}{2} + \frac{\Gamma_4}{2}\right)\mathbf{e}_2 \tag{2.100}$$

but

$$\mathbf{e}_1 = \frac{\mathbf{n}\times\mathbf{L}_3}{\|\mathbf{L}_3\|_2}, \quad \mathbf{e}_2 = -\frac{\mathbf{n}\times\mathbf{L}_1}{\|\mathbf{L}_1\|_2} \tag{2.101}$$

hence

$$\Delta\mathbf{V} = -\frac{\mathbf{n}\times\mathbf{L}_3}{2\,\|\mathbf{L}_1\|_2\,\|\mathbf{L}_3\|_2}(\Gamma_2+\Gamma_3) - \frac{\mathbf{n}\times\mathbf{L}_1}{2\,\|\mathbf{L}_1\|_2\,\|\mathbf{L}_3\|_2}(\Gamma_1+\Gamma_4) \tag{2.102}$$

but $\|\mathbf{L}_1\|_2\,\|\mathbf{L}_3\|_2 = A \simeq$ Area of the element, therefore

$$\Delta\mathbf{V} = -\mathbf{n}\times\left[(\Gamma_2+\Gamma_3)\,\mathbf{L}_3 + (\Gamma_1+\Gamma_4)\,\mathbf{L}_1\right]\frac{1}{2A} \tag{2.103}$$

Another interpretation of Equation (2.103) follows. To this end, let us introduce the vector

$\mathbf{\Gamma}$ as follows

$$\mathbf{\Gamma} = \frac{\Gamma_1}{2}\mathbf{L}_1 + \frac{\Gamma_2}{2}\mathbf{L}_2 + \frac{\Gamma_3}{2}\mathbf{L}_3 + \frac{\Gamma_4}{2}\mathbf{L}_4 \tag{2.104}$$

However, for a rectangular element $\mathbf{L}_4 = \mathbf{L}_1$ and $\mathbf{L}_2 = \mathbf{L}_3$, then

$$\mathbf{\Gamma} = \frac{1}{2}\left[\left(\Gamma_1 + \Gamma_4\right)\mathbf{L}_1 + \left(\Gamma_2 + \Gamma_3\right)\mathbf{L}_3\right] \tag{2.105}$$

and finally, $\Delta\mathbf{V}$ can be written as

$$\Delta\mathbf{V} = -\frac{\mathbf{n} \times \mathbf{\Gamma}}{A} \tag{2.106}$$

where the $A = \|\mathbf{L}_3 \times \mathbf{L}_1\|_2$.

Parallelogram Element

A typical parallelogram element is shown in Figure 2-28. For this case, $\Delta\mathbf{V}_1$ and $\Delta\mathbf{V}_2$ have the following expressions,

$$\Delta\mathbf{V}_1 = -\frac{1}{\|\mathbf{L}_1\|_2 \cos\Lambda}\left(\frac{\Gamma_2}{2} + \frac{\Gamma_3}{2}\right)\mathbf{e}_1 \tag{2.107}$$

$$\Delta\mathbf{V}_2 = \frac{1}{\|\mathbf{L}_3\|_2 \cos\Lambda}\left(\frac{\Gamma_1}{2} + \frac{\Gamma_4}{2}\right)\mathbf{e}_2 \tag{2.108}$$

where

$$\mathbf{e}_1 = \frac{\mathbf{n} \times \mathbf{L}_3}{\|\mathbf{L}_3\|_2}, \quad \mathbf{e}_2 = -\frac{\mathbf{n} \times \mathbf{L}_1}{\|\mathbf{L}_1\|_2} \tag{2.109}$$

hence

$$\Delta\mathbf{V} = \Delta\mathbf{V}_1 + \Delta\mathbf{V}_2$$

or

$$\Delta\mathbf{V} = -\frac{\mathbf{n} \times \mathbf{L}_3}{2\,\|\mathbf{L}_1\|_2\,\|\mathbf{L}_3\|_2 \cos\Lambda}\left(\Gamma_2 + \Gamma_3\right) - \frac{\mathbf{n} \times \mathbf{L}_1}{2\,\|\mathbf{L}_1\|_2\,\|\mathbf{L}_3\|_2 \cos\Lambda}\left(\Gamma_1 + \Gamma_4\right) \tag{2.110}$$

Now, let us consider the following cross product

$$\begin{aligned} \mathbf{L}_3 \times \mathbf{L}_1 &= \|\mathbf{L}_3\|_2\,\|\mathbf{L}_1\|_2 \sin\left(\frac{\pi}{2} + \Lambda\right) \\ &= \|\mathbf{L}_3\|_2\,\|\mathbf{L}_1\|_2 \cos\Lambda \\ &= A \simeq \text{ Area of the element} \end{aligned} \tag{2.111}$$

Therefore

$$\Delta\mathbf{V} = -\mathbf{n}\times\left[\left(\Gamma_2+\Gamma_3\right)\mathbf{L}_3+\left(\Gamma_1+\Gamma_4\right)\mathbf{L}_1\right]\frac{1}{2A} \tag{2.112}$$

General Case

A general element is shown in Figure 2-29. By defining the vector $\mathbf{\Gamma}$ as in the two previous sections we can evaluate the jump in tangential velocity across the vortex sheet as

$$\Delta\mathbf{V} = -\frac{\mathbf{n}\times\mathbf{\Gamma}}{A}$$

where A, an approximation to the area of the element, can be evaluated as follows

$$\begin{aligned} A &= A_1 + A_2 \\ &= \frac{1}{2}\left\|\mathbf{L}_1\times\mathbf{L}_3\right\|_2 + \frac{1}{2}\left\|\mathbf{L}_2\times\mathbf{L}_4\right\|_2 \end{aligned} \tag{2.113}$$

2.11.3 Evaluation of $\left.\frac{\partial\Phi}{\partial t}\right|_{\mathbf{R}_U} - \left.\frac{\partial\Phi}{\partial t}\right|_{\mathbf{R}_L}$

In this section we describe how the difference in these two derivatives is calculated. $\frac{\partial\Phi}{\partial t}\left(\mathbf{R},t\right)$ is defined as

$$\frac{\partial\Phi}{\partial t}\left(\mathbf{R},t\right) = \lim_{\Delta t\to 0}\frac{\Phi\left(\mathbf{R},t+\Delta t\right)-\Phi\left(\mathbf{R},t\right)}{\Delta t} \tag{2.114}$$

where $\mathbf{R}$ is a (fixed) position in the ground-fixed coordinate system. In our applications, it is rather difficult to evaluate $\frac{\partial\Phi}{\partial t}\left(\mathbf{R},t\right)$ directly and we find that it is convenient to replace $\Phi\left(\mathbf{R},t+\Delta t\right)$ with an expression involving $\Phi\left(\mathbf{R}+\Delta\mathbf{R},t+\Delta t\right)$ where, for the moment, $\Delta\mathbf{R}$ is arbitrary, but small. Then, expanding $\Phi\left(\mathbf{R},t\right)$ around $\mathbf{R}$ and t, we obtain

$$\Phi\left(\mathbf{R}+\Delta\mathbf{R},t+\Delta t\right) = \Phi\left(\mathbf{R},t\right) + \nabla\Phi\left(\mathbf{R},t\right)\cdot\Delta\mathbf{R} + \frac{\partial\Phi}{\partial t}\left(\mathbf{R},t\right)\ \Delta t + HOT \tag{2.115}$$

where the higher-order terms in the remainder (HOT) are given by

$$HOT = O\left(\left\|\Delta\mathbf{R}\right\|_2^2,\ \left\|\Delta\mathbf{R}\right\|_2\Delta t,\ \Delta t^2\right) \tag{2.116}$$

and O is the order symbol. Then it follows from (2.115) that

$$\frac{\partial \Phi}{\partial t}(\mathbf{R},t) = \frac{\Phi(\mathbf{R}+\Delta\mathbf{R},t+\Delta t)-\Phi(\mathbf{R},t)}{\Delta t} - \nabla\Phi(\mathbf{R},t)\cdot\frac{\Delta\mathbf{R}}{\Delta t} + \frac{1}{\Delta t}HOT \tag{2.117}$$

For our application a convenient choice for $\Delta\mathbf{R}$ is the displacement of a point fixed either just below or just above a control point in the moving lattice. By choosing $\Delta\mathbf{R}$ in this way, we convert $\Phi(\mathbf{R},t)$ into a function of t only; it is the velocity potential associated with a point that moves with the deforming lattice. In this case $\dfrac{\Delta\mathbf{R}}{\Delta t}$ = the velocity of this point fixed to the moving lattice + HOT.

This choice is represented in Figure 2-30. In this figure P represents the point attached to the moving lattice, and P' represents the point fixed in space at position $\mathbf{R}$ where $\dfrac{\partial\Phi}{\partial t}$ is to be evaluated. Initially P and P' coincide; then during the interval Δt, P moves through the displacement $\Delta\mathbf{R}$ to its new position $\mathbf{R}+\Delta\mathbf{R}$ as shown.

We can gain insight into the way $\dfrac{\partial\Phi}{\partial t}(\mathbf{R},t)$ is calculated by taking the limit of Equation (2.117) as $\Delta t \to 0$:

$$\begin{aligned}
\frac{\partial\Phi}{\partial t}(\mathbf{R},t) &= \lim_{\Delta t\to 0}\frac{\Phi(\mathbf{R}+\Delta\mathbf{R},t+\Delta t)-\Phi(\mathbf{R},t)}{\Delta t} \\
&- \lim_{\Delta t\to 0}\nabla\Phi(\mathbf{R},t)\cdot\frac{\Delta\mathbf{R}}{\Delta t} + \lim_{\Delta t\to 0} O\left(\frac{\|\Delta\mathbf{R}\|_2^2}{\Delta t},\ \|\Delta\mathbf{R}\|_2,\ \Delta t\right) \\
&= \left.\frac{Đ\Phi}{Đt}\right|_P - \nabla\Phi(\mathbf{R},t)\cdot\ {}^N\mathbf{V}^P(t)
\end{aligned} \tag{2.118}$$

where $\dfrac{Đ\Phi}{Đt}$ is the "substantial derivative" of $\Phi(\mathbf{R},t)$ following a point fixed to the moving lattice (not a fluid particle as in the usual use of this term), and ${}^N\mathbf{V}^P(t)$ is the velocity of the point fixed to the lattice. If we express ${}^N\mathbf{V}^P(t)$ in the body-fixed reference frame, i.e.,

$${}^N\mathbf{V}^P(t) = {}^N\mathbf{v}^B(t) + {}^B\dot{\mathbf{r}}^P(t) + {}^N\boldsymbol{\omega}^B(t)\times {}^B\mathbf{r}^P(t) \tag{2.119}$$

where ${}^N\mathbf{v}^B(t)$ is the absolute velocity of the origin of the B-frame, ${}^B\mathbf{r}^P(t)$ is the position of point P in the B-frame, ${}^B\dot{\mathbf{r}}^P(t)$ is the velocity of point P relative to the B-frame, and ${}^N\boldsymbol{\omega}^B(t)$ is the angular velocity of the B-frame. Substituting this expression for ${}^N\mathbf{V}^P(t)$ into Equation

(2.118) we obtain

$$\frac{\partial \Phi}{\partial t}(\mathbf{R},t) = \left.\frac{\text{Đ}\Phi}{\text{Đ}t}\right|_P - \nabla\Phi(\mathbf{R},t)\cdot\left[{}^N\mathbf{v}^B(t) + {}^B\dot{\mathbf{r}}^P(t) + {}^N\boldsymbol{\omega}^B(t)\times {}^B\mathbf{r}^P(t)\right] \tag{2.120}$$

The two points fixed to the moving lattice, one just above (U) and the other just below (L) the control point (CP) in Figure 2-31, have the same velocity as the control point itself. But, there is a discontinuity in the velocity of the air flowing across the vortex sheet; hence, the fluid velocities at these two points are different. Now, we can make use of Equation (2.120) to compute $\frac{\partial \Phi}{\partial t}(\mathbf{R}_U,t) - \frac{\partial \Phi}{\partial t}(\mathbf{R}_L,t)$ as follows:

$$\begin{aligned}\frac{\partial \Phi}{\partial t}(\mathbf{R}_U,t) - \frac{\partial \Phi}{\partial t}(\mathbf{R}_L,t) &= \frac{\text{Đ}}{\text{Đ}t}\left[\Phi(\mathbf{R}_U,t) - \Phi(\mathbf{R}_L,t)\right] \\ &- \left[\nabla\Phi(\mathbf{R}_U,t) - \nabla\Phi(\mathbf{R}_L,t)\right]\cdot {}^N\mathbf{V}^{CP}(t)\end{aligned} \tag{2.121}$$

but

$$\nabla\Phi(\mathbf{R}_U,t) = \mathbf{V}_U = \mathbf{V}_m + \frac{\Delta\mathbf{V}}{2}, \quad \nabla\Phi(\mathbf{R}_L,t) = \mathbf{V}_L = \mathbf{V}_m - \frac{\Delta\mathbf{V}}{2} \tag{2.122}$$

and, hence,

$$\nabla\Phi(\mathbf{R}_U,t) - \nabla\Phi(\mathbf{R}_L,t) = \Delta\mathbf{V} \tag{2.123}$$

Moreover, it follows from Figure 2-32 that $\Phi(\mathbf{R}_U,t) - \Phi(\mathbf{R}_L,t)$ can be computed as

$$\Phi(\mathbf{R}_U,t) - \Phi(\mathbf{R}_L,t) = \oint_{C(t)} \mathbf{V}\cdot d\mathbf{R} = \Gamma(t) \tag{2.124}$$

where $C(t)$ is a path that goes from the point on the lower side of the surface around the leading edge to the same point on the upper side of the surface. It follows from Stokes' theorem that $\Gamma(t)$ has the same value as the circulation $G(t)$ for the loop that encloses the control point; hence, at control point i (see Figure 2-33), we have:

$$\left[\frac{\partial \Phi}{\partial t}(\mathbf{R}_U,t) - \frac{\partial \Phi}{\partial t}(\mathbf{R}_L,t)\right]_i = \frac{\text{Đ}G_i(t)}{\text{Đ}t} - \Delta\mathbf{V}_i\cdot\left[{}^N\mathbf{v}^B(t) + {}^N\dot{\mathbf{r}}^i(t) + {}^N\boldsymbol{\omega}^B(t)\times {}^B\mathbf{r}^i(t)\right] \tag{2.125}$$

In our numerical procedure, the "substantial" derivative $\frac{\text{Đ}G_i(t)}{\text{Đ}t}$ is approximated by a first-

order finite-difference:

$$\frac{Ð G_i(t)}{Ð t} \simeq \frac{G_i(t) - G_i(t - \Delta t)}{\Delta t} \tag{2.126}$$

where Δt is the time step used to obtain the numerical solution.

2.12 The Aerodynamic Model for Bridge One

The roadbed is represented as a flat plate, which is the same representation used in the earlier work by Fung [6]. A plate is the aerodynamic equivalent of a sheet of vorticity. The discontinuity in the tangential component of vorticity associated with this sheet of vorticity and the time variation of the velocity potential produce a difference between, or a discontinuity in, the pressures on the upper and lower surfaces of the plate, which is responsible for the aerodynamic force.

The exact aerodynamic force and moment exerted on a plate in a uniform steady flow can be obtained by considering all the vorticity to be concentrated in a single discrete vortex at a distance of one quarter chord from the leading edge with a circulation that causes the no–penetration boundary condition to be satisfied only at a distance of three quarters chord from the leading edge; this is the so–called one–quarter/three–quarter rule.

In the present model, the plate is divided into a number of elements, or platelets. Each platelet should be small enough that the flow varies only slightly along the length of a given element so that it appears to be in a uniform flow. Also changes in time should be occurring on a scale that is slow compared to the time it takes a fluid particle to travel the length of a platelet.

The arrangement of the platelets that model the roadbed as well as a typical platelet (in the enlargement) are represented in Figure 2-34.

The velocity at point (X_P, Y_P) associated with a discrete vortex with a clockwise circulation G at point (X_V, Y_V) is given by

$$U\left(X_P, Y_P, t\right)\ \hat{\mathbf{n}}_1 + V\left(X_P, Y_P, t\right)\ \hat{\mathbf{n}}_2 = \frac{G(t)}{2\pi} \frac{\left[\left(Y_P - Y_V\right)\ \hat{\mathbf{n}}_1 - \left(X_P - X_V\right)\ \hat{\mathbf{n}}_2\right]}{\left[\left(X_P - X_V\right)^2 + \left(Y_P - Y_V\right)^2\right]} \tag{2.127}$$

The no–penetration boundary condition has the form

$$(\mathbf{V}_P + \mathbf{V}_\infty + \mathbf{V}_W - \mathbf{V}_S) \cdot \mathbf{n} = 0 \tag{2.128}$$

where $\mathbf{V}_P + \mathbf{V}_\infty + \mathbf{V}_W$ is the velocity of a fluid particle next to the plate associated with (1) the vortices in the plate, (2) the on–coming freestream, and (3) the vortices in the wake, respectively; $\mathbf{V}_S$ is the velocity of the surface of the plate (thus, the velocity of the fluid particle relative to the plate appears inside the parentheses) and $\mathbf{n}$ is a vector normal to the surface of the plate. The no–penetration condition is imposed at the control points of the roadbed. It follows from Figure 2-35 that at all points on the roadbed

$$\mathbf{V}_\infty \cdot \mathbf{n} = V_\infty \ \sin(\theta + \alpha) \tag{2.129}$$

where α is the angle of attack of the oncoming freestream and $V_\infty = \|\mathbf{V}_\infty\|_2$; that at all control points on the roadbed

$$\mathbf{V}_S\left(\xi_i, t\right) \cdot \mathbf{n}\left(\xi_i, t\right) = \dot{y} \ \cos\theta - \dot{\theta} \ \xi_i \tag{2.130}$$

and

$$\mathbf{V}_W\left(\xi_i, t\right) \cdot \mathbf{n}\left(\xi_i, t\right) = U_{Wi} \ \sin\theta + V_{Wi} \ \cos\theta \tag{2.131}$$

where ξ_i is the position of the control point of element i with respect to a coordinate system attached to the plate with its origin at A, and (U_{Wi}, V_{Wi}) are the components of the total velocity in the ground–fixed reference frame associated with the wake at the control point of element i.

At any time, the only unknowns are the Gs around the discrete vortices in the plate. To determine them, we rewrite the no–penetration condition, Equation (2.128), as

$$\mathbf{V}_P\left(\xi_i, t\right) \cdot \mathbf{n}\left(\xi_i, t\right) = \sum_{j=1}^{N} A_{ij} \ G_j\left(t\right) = \left[\mathbf{V}_S\left(\xi_i, t\right) - \mathbf{V}_W\left(\xi_i, t\right) - \mathbf{V}_\infty\right] \cdot \mathbf{n}\left(\xi_i, t\right) \tag{2.132}$$

Here, the coefficient A_{ij} represents the normal component of the velocity at the control point of the i-th element associated with unit circulation around the discrete vortex of the j-th element; Equation (2.127) is used to compute the A_{ij}. Since the roadbed is modeled as a rigid plate,

these coefficients do not depend on time.

The upper limit on the summation, N, is $NP+1$ where NP is the number of elements (or discrete vortices) in the plate. The range of i is from 1 to NP. The additional equation is the requirement that the circulation around the path that encloses the plate and its wake remain zero. In addition to the unknown circulations around the vortices in each element, there is a "starting vortex" that forms at each time step, at the trailing edge. This is needed to satisfy the requirement that circulation be conserved. To satisfy the requirement that Δp vanish at the trailing edge, this vortex is convected away from the plate at the local particle velocity.

The generalized aerodynamic forces per unit span, $Q_y(t)$ and $Q_\theta(t)$, have the following form:

$$Q_y(t) = \left(\int_0^C \Delta p(\xi, t)\, d\xi \right) \cos\theta \tag{2.133}$$

$$Q_\theta(t) = -\int_0^C \xi\, \Delta p(\xi, t)\, d\xi \tag{2.134}$$

where C is the chord (width) of the bridge, Δp is the difference between the pressures on the upper and lower surfaces and ξ gives the position of points on the lifting surface (roadbed) relative to the center point A (see Figure 2-35). In the numerical model, these loads are computed by approximating the integrals in Equations (2.133) and (2.134) with finite sums. The difference in pressure on each element is obtained from the unsteady version of Bernoulli's equation (2.93). In this example Equation (2.93) can be rewritten as follows

$$(C_p)_L - (C_p)_U = \frac{P_L - P_U}{\frac{1}{2}\rho V_\infty^2} = \frac{\Delta p}{\frac{1}{2}\rho V_\infty^2} \tag{2.135}$$

$$= \frac{2}{V_\infty^2}\left[\frac{\partial}{\partial t}(\Phi_U - \Phi_L) - (\mathbf{V}_S - \mathbf{V}_{MEAN}) \cdot \Delta\mathbf{V} \right] \tag{2.136}$$

where $\Delta\mathbf{V} = \mathbf{V}_U - \mathbf{V}_L$ and $\mathbf{V}_{MEAN} = \frac{1}{2}(\mathbf{V}_U + \mathbf{V}_L) = \frac{1}{2}(\mathbf{V}_W + \mathbf{V}_\infty)$. The difference in the velocity, $\Delta\mathbf{V}$, is tangent to the plate and for element i is given by

$$\Delta\mathbf{V}_i = \frac{G_i}{\Delta\xi_i}\hat{\mathbf{t}} \tag{2.137}$$

where $\Delta\xi_i$ is the length of the platelet and $\hat{\mathbf{t}}$ is the unit vector tangent to the plate. For flat

plates the tangential component of $\mathbf{V}_{MEAN}$ is the sum of contributions from the freestream and the wake.

Taking into account Equations (2.124)-(2.126) and (2.137), one can now write Equation (2.136) as

$$\Delta C_p\left(\xi_i,t\right)=\frac{\Delta p\left(\xi_i,t\right)}{\frac{1}{2}\rho V_\infty^2}\cong\frac{2}{V_\infty^2}\left[\sum_{j=1}^{i}\frac{G_j\left(t\right)-G_j\left(t-\Delta t\right)}{\Delta t}+\frac{G_i\left(\mathbf{V}_{MEAN}-\mathbf{V}_S\right)\cdot\hat{\mathbf{t}}}{\Delta\xi_i}\right] \tag{2.138}$$

where

$$\mathbf{V}_S\cdot\hat{\mathbf{t}}=\dot{y}\sin\theta \tag{2.139}$$

The generalized forces in Equations (2.133) and (2.134) can now be written as

$$Q_y\left(t\right)\simeq\frac{1}{2}\rho V_\infty^2\left[\sum_{i=1}^{NP}\Delta C_p\left(\xi_i,t\right)\ \Delta\xi_i\cos\theta\right] \tag{2.140}$$

$$Q_\theta\left(t\right)\simeq-\frac{1}{2}\rho V_\infty^2\left[\sum_{i=1}^{NP}\xi_i\ \Delta C_p\left(\xi_i,t\right)\ \Delta\xi_i\right] \tag{2.141}$$

where ξ_i is the moment arm for element i.

2.13 The Aerodynamic Model for Bridge Two

Both the roadbed and wing are represented as flat plates. In the present model, the plates representing the roadbed and the wing are divided into a number of elements, or platelets. The arrangements of the platelets that model both the roadbed and the wing as well as a typical platelet (in the enlargement) are represented in Figure 2-36. The discrete vortices that model the wakes are also represented.

The no–penetration boundary condition has the form

$$\left(\mathbf{V}_P+\mathbf{V}_\infty+\mathbf{V}_W-\mathbf{V}_S\right)\cdot\mathbf{n}=0 \tag{2.142}$$

where $\mathbf{V}_P+\mathbf{V}_\infty+\mathbf{V}_W$ is the velocity of a fluid particle next to the plate generated by (1) the vortices in both plates, (2) the on–coming freestream, and (3) the vortices in both wakes,

respectively; $\mathbf{V}_S$ is the velocity of the surface of the plate and $\mathbf{n}$ is a vector normal to the surface of the plate. The no–penetration condition is imposed simultaneously and interactively at the control points of both the bridge and the wing. It follows from Figure 2-37 that at all points on the roadbed

$$\mathbf{V}_\infty \cdot \mathbf{n} = V_\infty \ \sin(\theta + \alpha) \tag{2.143}$$

where α is the angle of attack of the oncoming freestream, and $V_\infty = \|\mathbf{V}_\infty\|_2$; that at all control points on the roadbed

$$\mathbf{V}_S\left(\xi_i, t\right) \cdot \mathbf{n}\left(\xi_i, t\right) = \dot{y} \ \cos\theta - \dot{\theta} \ \xi_i \tag{2.144}$$

and

$$\mathbf{V}_W\left(\xi_i, t\right) \cdot \mathbf{n}\left(\xi_i, t\right) = U_{Wi} \ \sin\theta + V_{Wi} \ \cos\theta \tag{2.145}$$

where ξ_i is the position of the control point of element i with respect to a coordinate system attached to the roadbed with its origin at A, and (U_{Wi}, V_{Wi}) are the components of the total velocity in the ground–fixed reference frame associated with both wakes at the control point of element i. At all points on the wing,

$$\mathbf{V}_\infty \cdot \mathbf{n} = V_\infty \ \sin\left(\alpha + \theta + \delta\right) \tag{2.146}$$

where $\delta\left(t\right)$ is the angular deflection of the wing relative to the roadbed; at all control points on the wing,

$$\mathbf{V}_S\left(\eta_j, t\right) \cdot \mathbf{n}\left(\eta_j, t\right) = \dot{y} \ \cos\left(\theta + \delta\right) - h \ \dot{\theta} \ \sin\delta - \eta_j \ \left(\dot{\theta} + \dot{\delta}\right) \tag{2.147}$$

and

$$\mathbf{V}_W\left(\eta_j, t\right) \cdot \mathbf{n}\left(\eta_j, t\right) = U_{Wj} \ \sin\left(\theta + \delta\right) + V_{Wj} \ \cos\left(\theta + \delta\right) \tag{2.148}$$

where η_j is the position of the control point of element j with respect to a coordinate system attached to wing one with its origin at B, and (U_{Wj}, V_{Wj}) are the components of the total velocity in the ground–fixed reference frame associated with both wakes at the control point of element j.

At any time, the only unknowns are the Gs around the discrete vortices in the plates. To

determine them, we rewrite the no–penetration condition, Equation (2.142), as

$$\begin{aligned} \mathbf{V}_P(\xi_i,t)\cdot\mathbf{n}(\xi_i,t) &= \sum_{l=1}^{N} A_{il}(t)\ G_l(t) \\ &= [\mathbf{V}_S(\xi_i,t)-\mathbf{V}_W(\xi_i,t)-\mathbf{V}_\infty]\cdot\mathbf{n}(\xi_i,t) \end{aligned} \tag{2.149}$$

$$\begin{aligned} \mathbf{V}_P\left(\eta_j,t\right)\cdot\mathbf{n}\left(\eta_j,t\right) &= \sum_{l=1}^{N} A_{jl}(t)\ G_l(t) \\ &= \left[\mathbf{V}_S\left(\eta_j,t\right)-\mathbf{V}_W\left(\eta_j,t\right)-\mathbf{V}_\infty\right]\cdot\mathbf{n}\left(\eta_j,t\right) \end{aligned} \tag{2.150}$$

Here, $i=1,2,\ldots,NP1$, $j=1,2,\ldots,NP2$, and the upper limit on the summations, N, is $NP1+NP2+2$ where $NP1$ and $NP2$ are the number of elements (or discrete vortices) in the models of the roadbed and the wing, respectively. The two additional equations are the requirement that the circulations around the paths that enclose each plate and its wake remain zero. In addition to the unknown circulations around the vortices in each element, there are two "starting vortices" that form at each time step, one at each trailing edge. These must convect with the local fluid particle in order to satisfy the requirement that Δp vanish at the trailing edges (i.e. the Kutta condition).

The coefficient $A_{mn}(t)$ represents the normal component of the velocity at the control point of the m-th element associated with unit circulation around the discrete vortex of the n-th element; Equation (2.127) is used to compute the $A_{mn}(t)$. The matrix $A_{mn}(t)$ has four distinct sectors: one gives the influence of the bridge on itself, one gives the influence of the wing on itself, one gives the influence of the bridge on the wing, and one gives the influence of the wing on the bridge. In general, because the wing moves relative to the bridge, the last two sectors must be re–computed at each time step.

The generalized aerodynamic forces per unit span, $Q_y(t)$ and $Q_\theta(t)$, have the following form:

$$Q_y(t)=\left(\int_0^{C_B}\Delta p(\xi,t)\ d\xi\right)\cos\theta+\left(\int_0^{C_W}\Delta p(\eta,t)\ d\eta\right)\cos(\theta+\delta) \tag{2.151}$$

$$Q_\theta(t)=-\int_0^{C_B}\xi\ \Delta p(\xi,t)\ d\xi-\int_0^{C_W}\eta\ \Delta p(\eta,t)\ d\eta-\left(\int_0^{C_W}\Delta p(\eta,t)\ d\eta\right)h\sin\delta \tag{2.152}$$

where C_B and C_W are the chords (widths) of the bridge and wing, Δp is the difference

between the pressures on the upper and lower surfaces of lifting surfaces (roadbed and wing), h is the distance between the bridge and the airfoil (see Figure 2-37), ξ gives the position of points on the roadbed relative to its center point (i.e. point A), and η gives the position of points on the wing relative to its center point (i.e. point B). In the numerical model, these loads are computed by approximating the integrals in Equations (2.151) and (2.152) with finite sums. As in the previous section, the difference in pressure on each element is obtained from the unsteady Bernoulli equation. The difference in the pressures on the upper and lower surfaces of the plate is given by Equation (2.136), but taking into account that for this particular example, $\mathbf{V}_{MEAN}$ is the sum of contributions from the other plate, the freestream, and both wakes. Moreover, for the wing, Equation (2.139) must be modified as follows:

$$\mathbf{V}_S \cdot \hat{\mathbf{t}} = \dot{y}\ \sin(\theta + \delta) - h\ \dot{\theta}\ \cos\theta \tag{2.153}$$

where $\hat{\mathbf{t}}$ is a unit vector tangent to the wing.

The generalized forces in Equations (2.151) and (2.152) can now be written as

$$Q_y(t) \simeq \frac{1}{2}\rho V_\infty^2 \left[\left(\sum_{i=1}^{NP1} \Delta C_p(\xi_i, t)\ \Delta\xi_i \right) \cos\theta + \left(\sum_{j=1}^{NP2} \Delta C_p\left(\eta_j, t\right)\ \Delta\eta_j \right) \cos(\theta + \delta) \right] \tag{2.154}$$

$$Q_\theta(t) \simeq -\frac{1}{2}\rho V_\infty^2 \left[\sum_{i=1}^{NP1} \xi_i\ \Delta C_p(\xi_i, t)\ \Delta\xi_i + \left(\sum_{j=1}^{NP2} \Delta C_p\left(\eta_j, t\right)\ \Delta\eta_j \right) h\ \sin\delta \right] \tag{2.155}$$

where ξ_i is the moment arm for element i on the roadbed, $\Delta\xi_i$ is its length, η_j is the moment arm for element j on the wing, and $\Delta\eta_j$ is its length.

2.14 The Aerodynamic Model for Bridge Three

All three, the roadbed, wing one, and wing two, are represented as flat plates. In the present model, the plates representing the roadbed and the wings are divided into a number of elements, or platelets. The arrangements of the platelets that model the roadbed and the wings are represented in Figure 2-38. The discrete vortices that model the wakes are also represented.

The no–penetration boundary condition has the form given by Equation (2.142). This boundary condition is imposed simultaneously and interactively at the control points of the

bridge and the wings. It follows from Figure 2-39 that at all points on the roadbed

$$\mathbf{V}_\infty \cdot \mathbf{n} = V_\infty \ \sin(\theta + \alpha) \tag{2.156}$$

where α is the angle of attack of the oncoming freestream, and $V_\infty = \|\mathbf{V}_\infty\|_2$; that at all control points on the roadbed

$$\mathbf{V}_S(\xi_i, t) \cdot \mathbf{n}(\xi_i, t) = \dot{y} \ \cos\theta - \dot{\theta} \ \xi_i \tag{2.157}$$

and

$$\mathbf{V}_W(\xi_i, t) \cdot \mathbf{n}(\xi_i, t) = U_{Wi} \ \sin\theta + V_{Wi} \ \cos\theta \tag{2.158}$$

where ξ_i is the position of the control point of element i with respect to a coordinate system attached to the roadbed with its origin at A, and (U_{Wi}, V_{Wi}) are the components of the total velocity in the ground–fixed reference frame associated with all three wakes at the control point of element i. At all points on wing one (see Figure 2-39),

$$\mathbf{V}_\infty \cdot \mathbf{n} = V_\infty \ \sin(\alpha + \theta + \delta_1) \tag{2.159}$$

where $\delta_1(t)$ is the angular deflection of wing one relative to the roadbed; at all control points on wing one,

$$\begin{aligned} \mathbf{V}_S\left(\eta_j, t\right) \cdot \mathbf{n}\left(\eta_j, t\right) &= \dot{y} \ \cos(\theta + \delta_1) + [L + \ell_1 \sin\beta_1] \cos\delta_1 \ \dot{\theta} \\ &- \ell_1 \cos\beta_1 \sin\delta_1 \ \dot{\theta} - \eta_j \ \left(\dot{\theta} + \dot{\delta}_1\right) \end{aligned} \tag{2.160}$$

and

$$\mathbf{V}_W\left(\eta_j, t\right) \cdot \mathbf{n}\left(\eta_j, t\right) = U_{Wj} \ \sin(\theta + \delta_1) + V_{Wj} \ \cos(\theta + \delta_1) \tag{2.161}$$

where η_j is the position of the control point of element j with respect to a coordinate system attached to wing one with its origin at B, and (U_{Wj}, V_{Wj}) are the components of the total velocity in the ground–fixed reference frame associated with all three wakes at the control point of element j. At all points on wing two (see Figure 2-39),

$$\mathbf{V}_\infty \cdot \mathbf{n} = V_\infty \ \sin(\alpha + \theta + \delta_2) \tag{2.162}$$

where $\delta_2(t)$ is the angular deflection of wing two relative to the roadbed; at all control points on wing two,

$$\begin{aligned}\mathbf{V}_S(\zeta_k,t)\cdot\mathbf{n}(\zeta_k,t) &= \dot{y}\ \cos(\theta+\delta_2) - [L+\ell_2\sin\beta_2]\cos\delta_2\ \dot{\theta} \\ &- \ell_2\cos\beta_2\sin\delta_2\ \dot{\theta} - \zeta_k\ \left(\dot{\theta}+\dot{\delta}_2\right)\end{aligned} \tag{2.163}$$

and

$$\mathbf{V}_W(\zeta_k,t)\cdot\mathbf{n}(\zeta_k,t) = U_{Wk}\ \sin(\theta+\delta_2) + V_{Wk}\ \cos(\theta+\delta_2) \tag{2.164}$$

where ζ_k is the position of the control point of element k with respect to a coordinate system attached to wing two with its origin at C, and (U_{Wk}, V_{Wk}) are the components of the total velocity in the ground–fixed reference frame associated with all three wakes at the control point of element k.

At any time, the only unknowns are the Gs around the discrete vortices in the plates. To determine them, we rewrite the no–penetration condition, Equation (2.142), as

$$\begin{aligned}\mathbf{V}_P(\xi_i,t)\cdot\mathbf{n}(\xi_i,t) &= \sum_{l=1}^{N} A_{il}(t)\ G_l(t) \\ &= [\mathbf{V}_S(\xi_i,t) - \mathbf{V}_W(\xi_i,t) - \mathbf{V}_\infty]\cdot\mathbf{n}(\xi_i,t)\end{aligned} \tag{2.165}$$

$$\begin{aligned}\mathbf{V}_P\left(\eta_j,t\right)\cdot\mathbf{n}\left(\eta_j,t\right) &= \sum_{l=1}^{N} A_{jl}(t)\ G_l(t) \\ &= \left[\mathbf{V}_S\left(\eta_j,t\right) - \mathbf{V}_W\left(\eta_j,t\right) - \mathbf{V}_\infty\right]\cdot\mathbf{n}\left(\eta_j,t\right)\end{aligned} \tag{2.166}$$

$$\begin{aligned}\mathbf{V}_P(\zeta_k,t)\cdot\mathbf{n}(\zeta_k,t) &= \sum_{l=1}^{N} A_{kl}(t)\ G_l(t) \\ &= [\mathbf{V}_S(\zeta_k,t) - \mathbf{V}_W(\zeta_k,t) - \mathbf{V}_\infty]\cdot\mathbf{n}(\zeta_k,t)\end{aligned} \tag{2.167}$$

Here, $i = 1,2,\ldots,NPB$, $j = 1,2,\ldots,NPW1$, $k = 1,2,\ldots,NPW2$, and the upper limit on the summations, N, is $NPB + NPW1 + NPW2 + 3$ where NPB, $NPW1$, and $NPW2$ are the numbers of elements (or discrete vortices) in the models of the roadbed, wing one, and wing two respectively. The three additional equations are the requirement that the circulations around the paths that enclose each plate and its wake remain zero. In addition to the unknown

circulations around the vortices in each element, there are three "starting vortices" that form at each time step, one at each trailing edge. These must convect with the local fluid particle in order to satisfy the Kutta condition.

The matrix $A_{mn}(t)$ has nine distinct sectors that give the influence of the roadbed on itself and on the wings, and to give the influence of the wings on themselves and on the roadbed. In general, because the wings move relative to the bridge, six of those sectors must be re–computed at each time step. Equation (2.127) is used to compute the $A_{mn}(t)$.

The generalized aerodynamic forces per unit span, Q_y^A, Q_θ^A, $Q_{\delta_1}^A$, and $Q_{\dot{\delta}_1}^A$ have the following form:

$$\begin{aligned} Q_y^A(t) &= \left[\int_0^{C_B} \Delta p(\xi,t)\ d\xi\right]\cos\theta \\ &+ \left[\int_0^{C_{W1}} \Delta p(\eta,t)\ d\eta\right]\cos(\theta+\delta_1) \\ &+ \left[\int_0^{C_{W2}} \Delta p(\zeta,t)\ d\zeta\right]\cos(\theta+\delta_2) \end{aligned} \tag{2.168}$$

$$\begin{aligned} Q_\theta^A(t) &= -\int_0^{C_B} \xi\ \Delta p(\xi,t)\ d\xi - \int_0^{C_{W1}} \eta\ \Delta p(\eta,t)\ d\eta - \int_0^{C_{W2}} \zeta\ \Delta p(\zeta,t)\ d\zeta \\ &+ \left[\int_0^{C_{W1}} \Delta p(\eta,t)\ d\eta\right]\{[L+\ell_1\sin\beta_1)]\cos\delta_1 - \ell_1\cos\beta_1\sin\delta_1\} \\ &- \left[\int_0^{C_{W2}} \Delta p(\zeta,t)\ d\zeta\right]\{[L+\ell_2\sin\beta_2)]\cos\delta_2 + \ell_2\cos\beta_2\sin\delta_2\} \end{aligned} \tag{2.169}$$

$$Q_{\delta_1}^A(t) = -\int_0^{C_{W1}} \eta\ \Delta p(\eta,t)\ d\eta \tag{2.170}$$

$$Q_{\delta_2}^A(t) = -\int_0^{C_{W2}} \zeta\ \Delta p(\zeta,t)\ d\zeta \tag{2.171}$$

where C_B, C_{W1}, and C_{W2} are the chords (widths) of the bridge, wing one, and wing two respectively, Δp is the difference between the pressures on the upper and lower surfaces of lifting surfaces (roadbed and wings), $\ell_1\cos\beta_1$ is the distance between the bridge and wing one, $\ell_2\cos\beta_2$ is the distance between the bridge and wing two, ξ gives the position of points on the bridge relative to point A, η gives the position of points on wing one relative to point B, and ζ

gives the position of points on wing two relative to point C (see Figure 2-39). In the numerical model, these loads are computed by approximating the integrals in Equations (2.168)-(2.171) with finite sums.

As in the two previous sections, the difference in pressure on each element is obtained from the unsteady Bernoulli equation. The difference in the pressures on the upper and lower surfaces of the plates is given by Equation (2.136), but for this particular example, $\mathbf{V}_{MEAN}$ is the sum of contributions from the two other plates, the freestream, and all three wakes. By repeating the procedure followed above, we can now write the generalized forces in Equations (2.168)-(2.171) as

$$\begin{aligned} Q_y^A(t) &= \left(\sum_{i=1}^{NPB} N_i\right)\cos\theta + \left(\sum_{j=1}^{NPW1} N_j\right)\cos(\theta+\delta_1) \\ &+ \left(\sum_{k=1}^{NPW2} N_k\right)\cos(\theta+\delta_2) \end{aligned} \tag{2.172}$$

$$\begin{aligned} Q_\theta^A(t) &= -\sum_{i=1}^{NPB} N_i\xi_i - \sum_{j=1}^{NPW1} N_j\eta_j - \sum_{k=1}^{NPW2} N_k\zeta_k \\ &+ \left(\sum_{j=1}^{NPW1} N_j\right)\left[L\cos\delta_1 + \ell_1\sin(\beta_1-\delta_1)\right] \\ &- \left(\sum_{k=1}^{NPW2} N_k\right)\left[L\cos\delta_2 + \ell_2\sin(\beta_2-\delta_2)\right] \end{aligned} \tag{2.173}$$

$$Q_{\delta_1}^A(t) = -\sum_{j=1}^{NPW1} N_j\ \eta_j \tag{2.174}$$

$$Q_{\delta_2}^A(t) = -\sum_{k=1}^{NPW2} N_k\ \zeta_k \tag{2.175}$$

where ξ_i is the moment arm for element i on the roadbed, η_j is the moment arm for element j on wing one, ζ_k is the moment arm for element k on wing two, and N_l is the normal force on element number l.

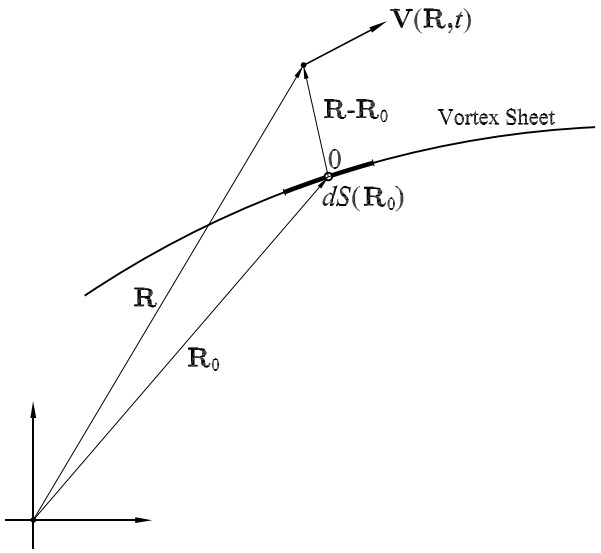

Figure 2-1: Velocity field $\mathbf{V}(\mathbf{R}, t)$ associated with a vortex sheet.

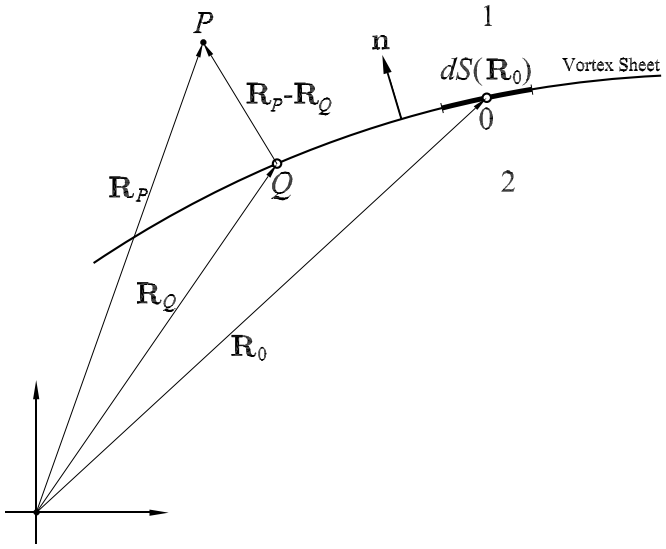

Figure 2-2: Sketch of coordinates for a vortex sheet.

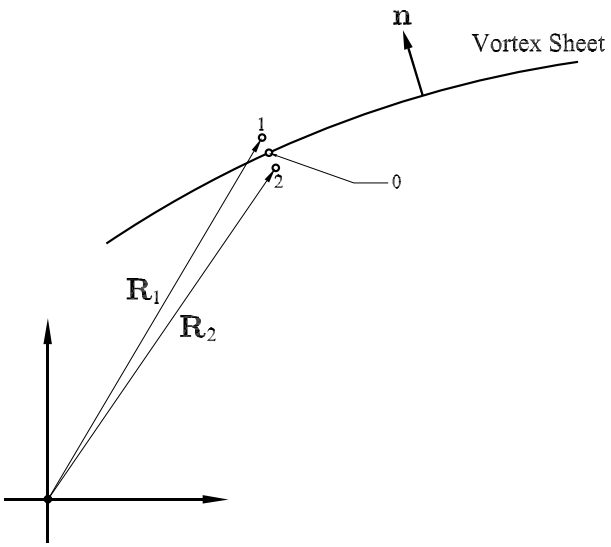

Figure 2-3: The jump $\mathbf{V}_2^1$ in the tangential velocity across a vortex sheet.

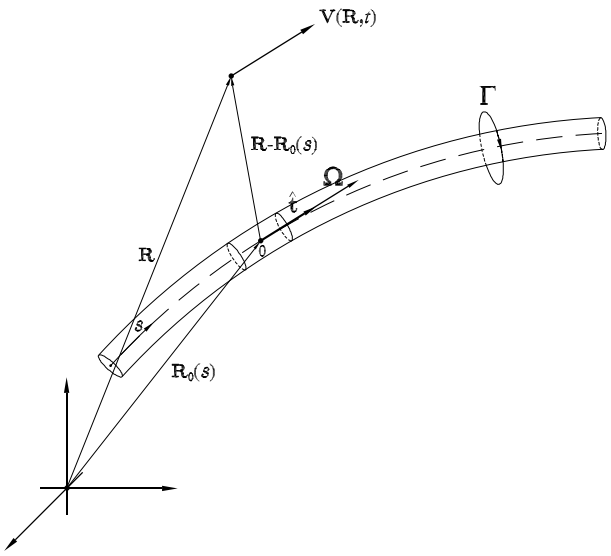

Figure 2-4: Vortex filament.

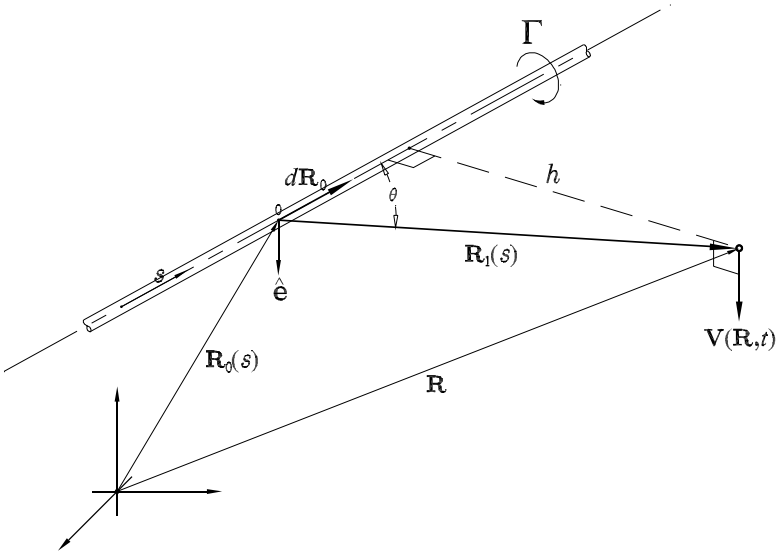

Figure 2-5: Inifinitely long straight line vortex.

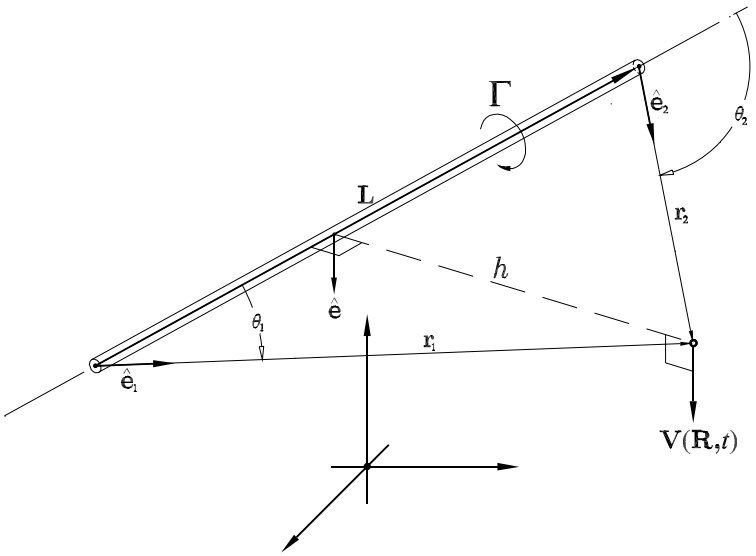

Figure 2-6: The Biot-Savart law.

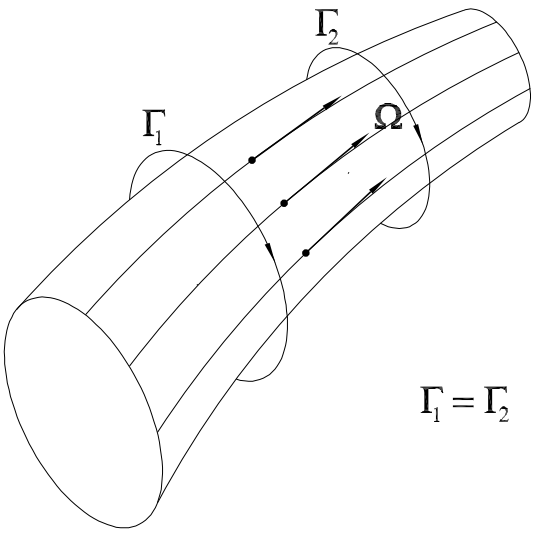

Figure 2-7: Vortex tube.

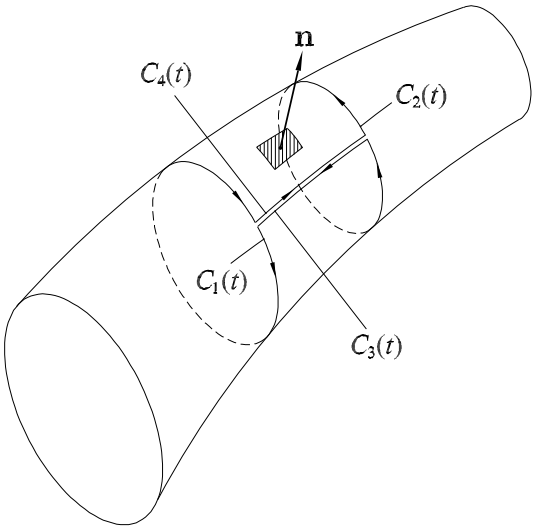

Figure 2-8: Proof of Helmholtz's first vortex theorem.

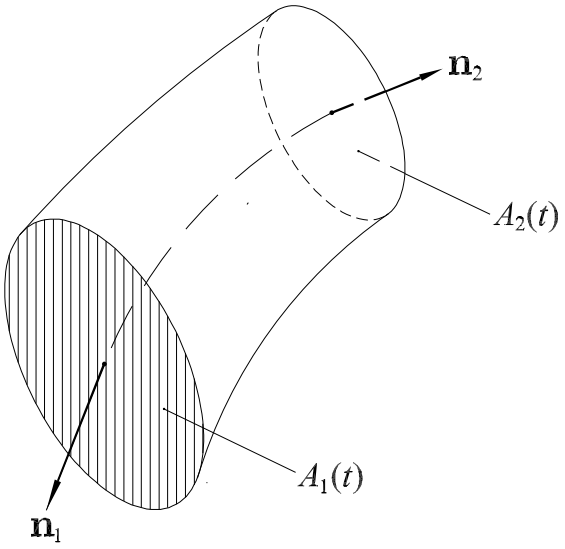

Figure 2-9: An alternative proof of Helmholtz's first vortex theorem.

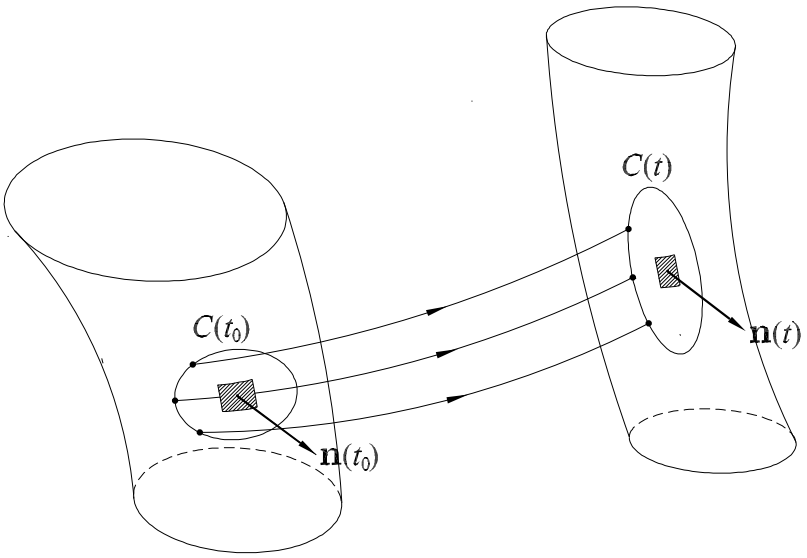

Figure 2-10: Helmholtz's second vortex theorem.

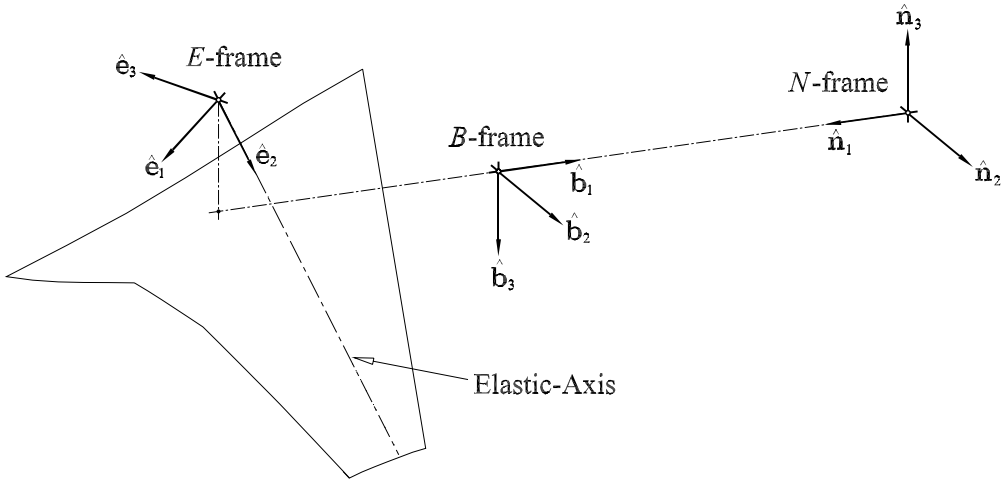

Figure 2-11: Coordinate systems for the aircraft.

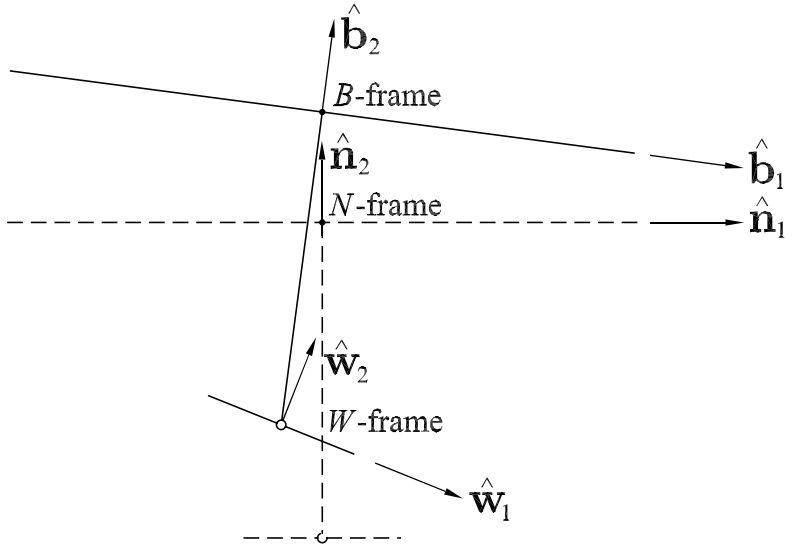

Figure 2-12: Coordinate systems for bridges

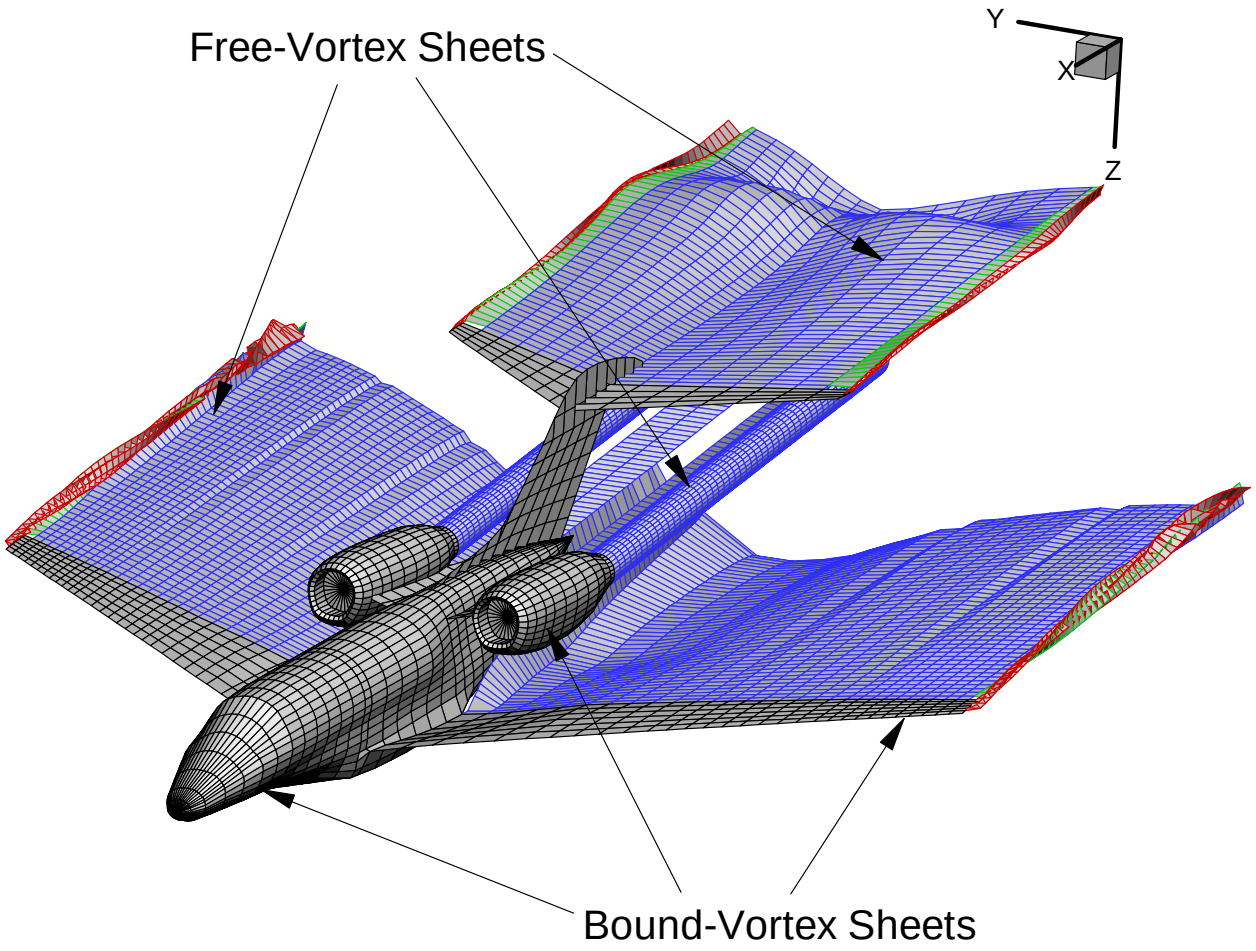

Figure 2-13: Bound and Free-Vortex Sheets

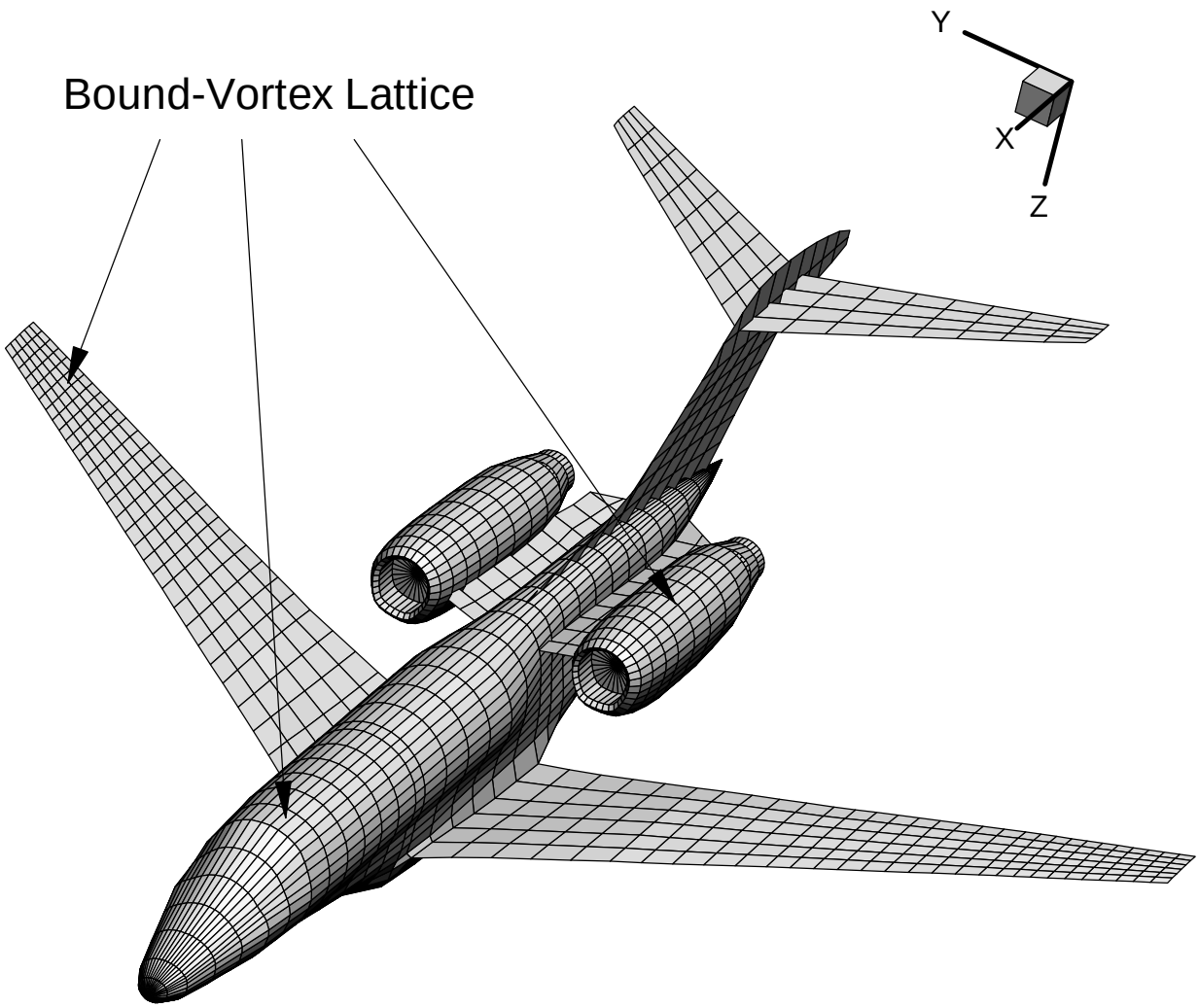

Figure 2-14: Bound-Vortex Lattice

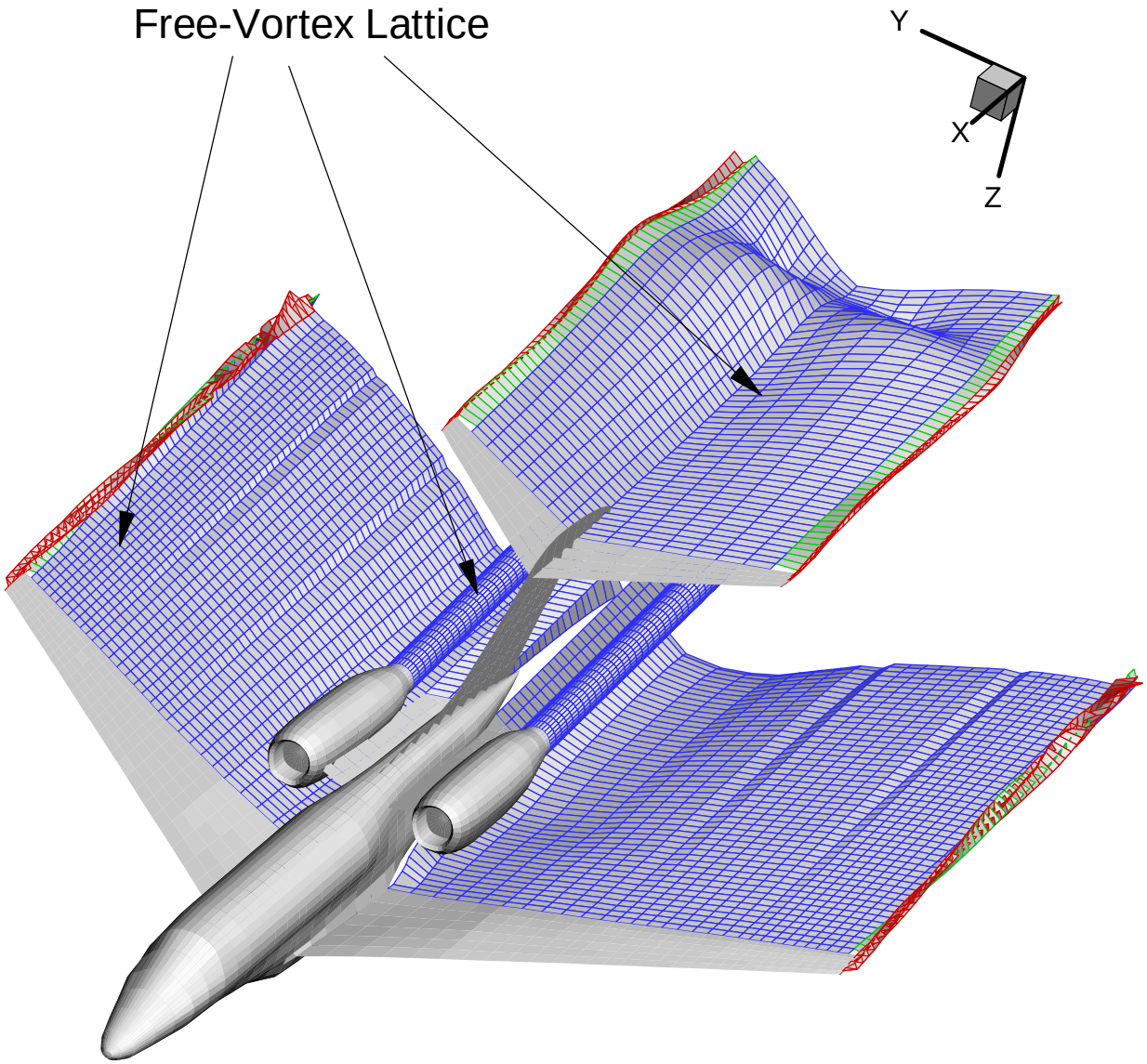

Figure 2-15: Free-Vortex Lattice

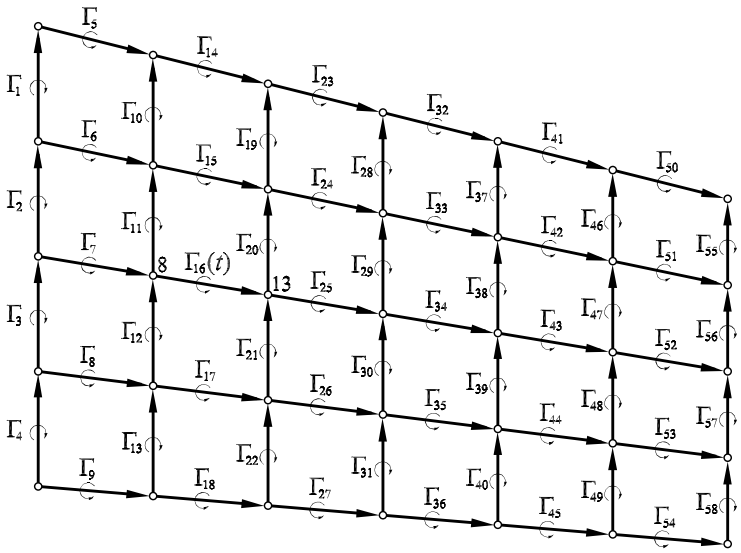

Figure 2-16: A portion of the lattice

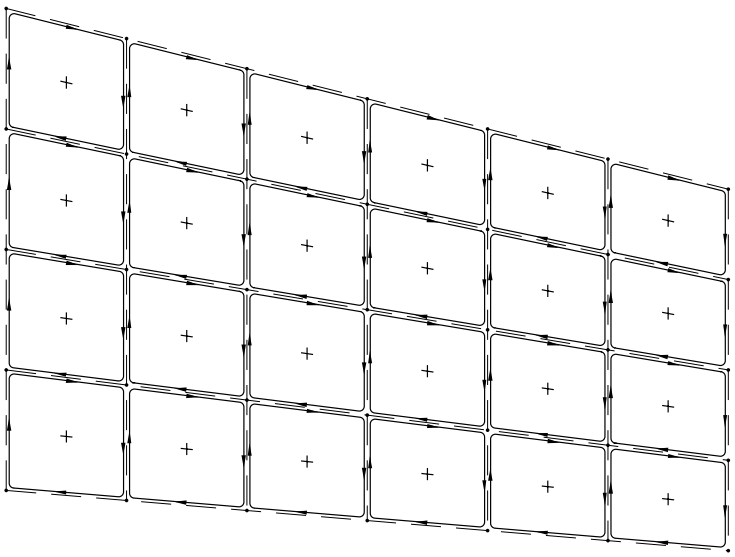

Figure 2-17: Closed loops of vortex segments.

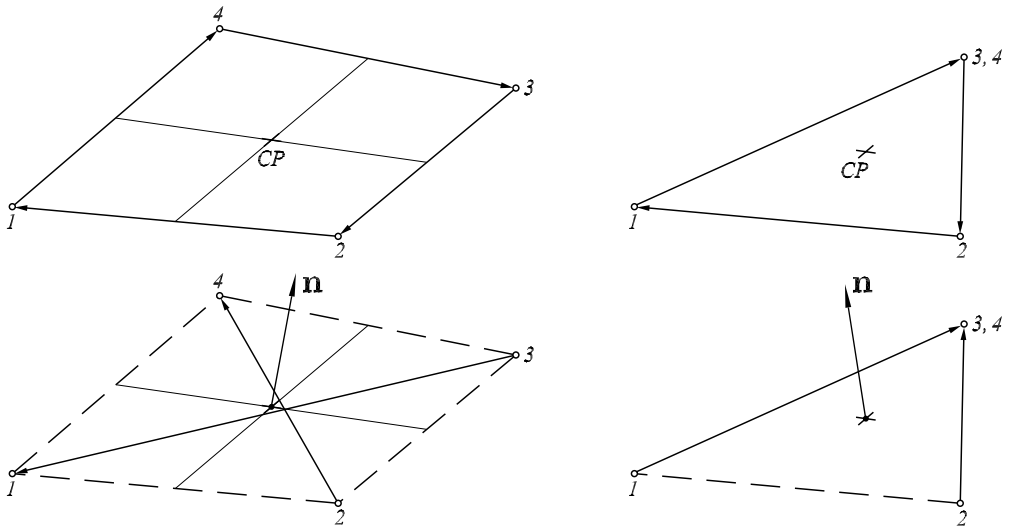

Figure 2-18: Typical four-sided and triangular elements.

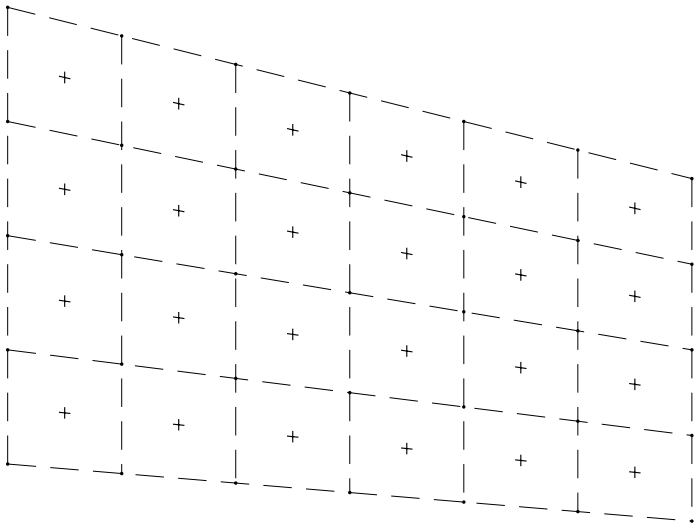

Figure 2-19: A lattice of 4×6 elements.

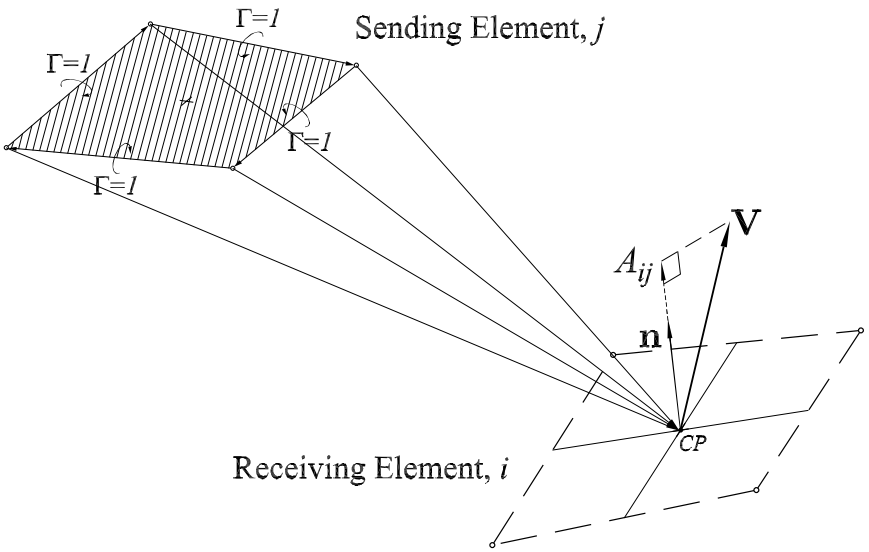

Figure 2-20: Geometric interpretation of the coefficients $A_{ij}(t)$.

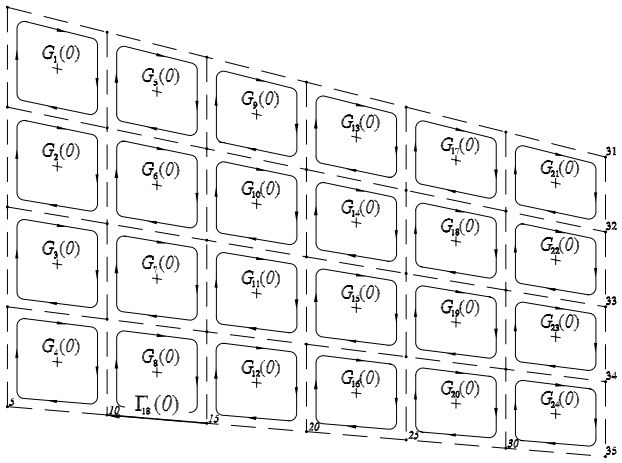

Figure 2-21: The solution at $t = 0$.

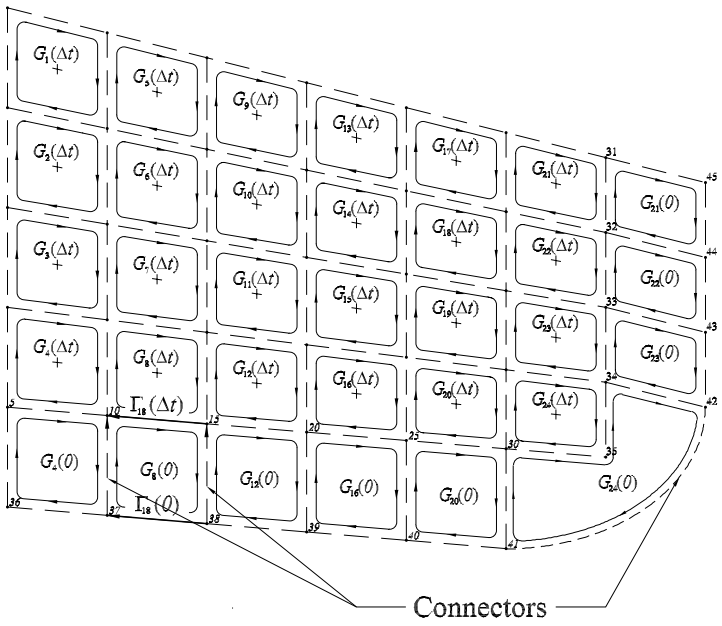

Figure 2-22: The solution at $t = \Delta t$.

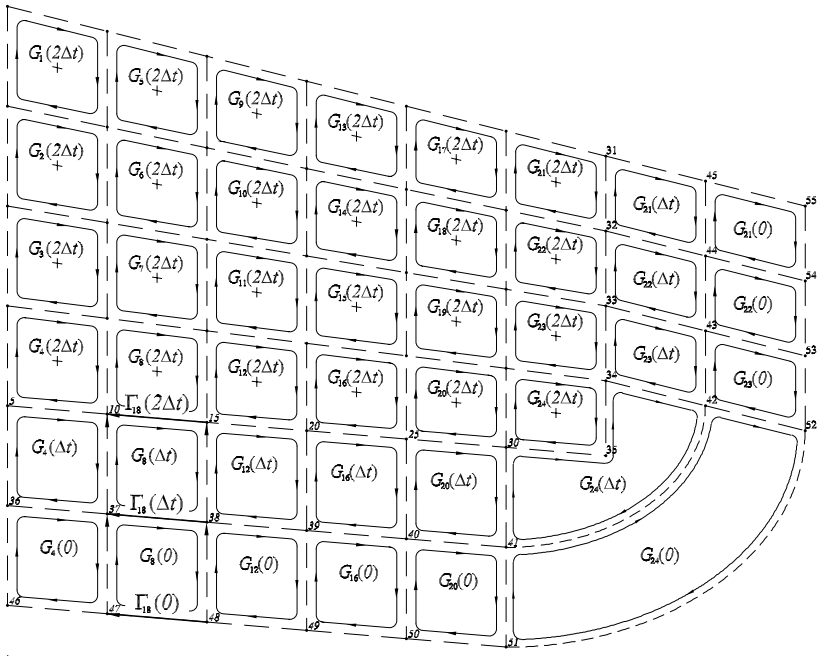

Figure 2-23: The solution at $t = 2\Delta t$.

5 Time Steps

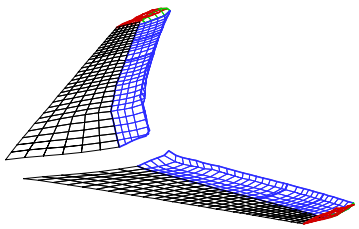

10 Time Steps

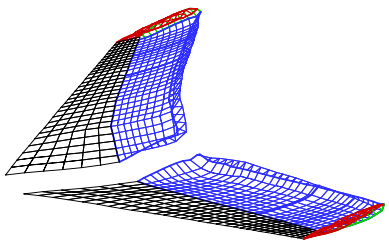

15 Time Steps

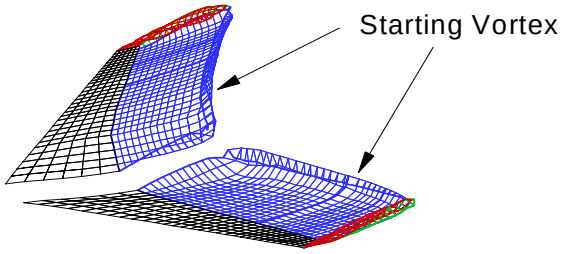

Figure 2-24: The solutions after 5, 10, and 15 time steps.

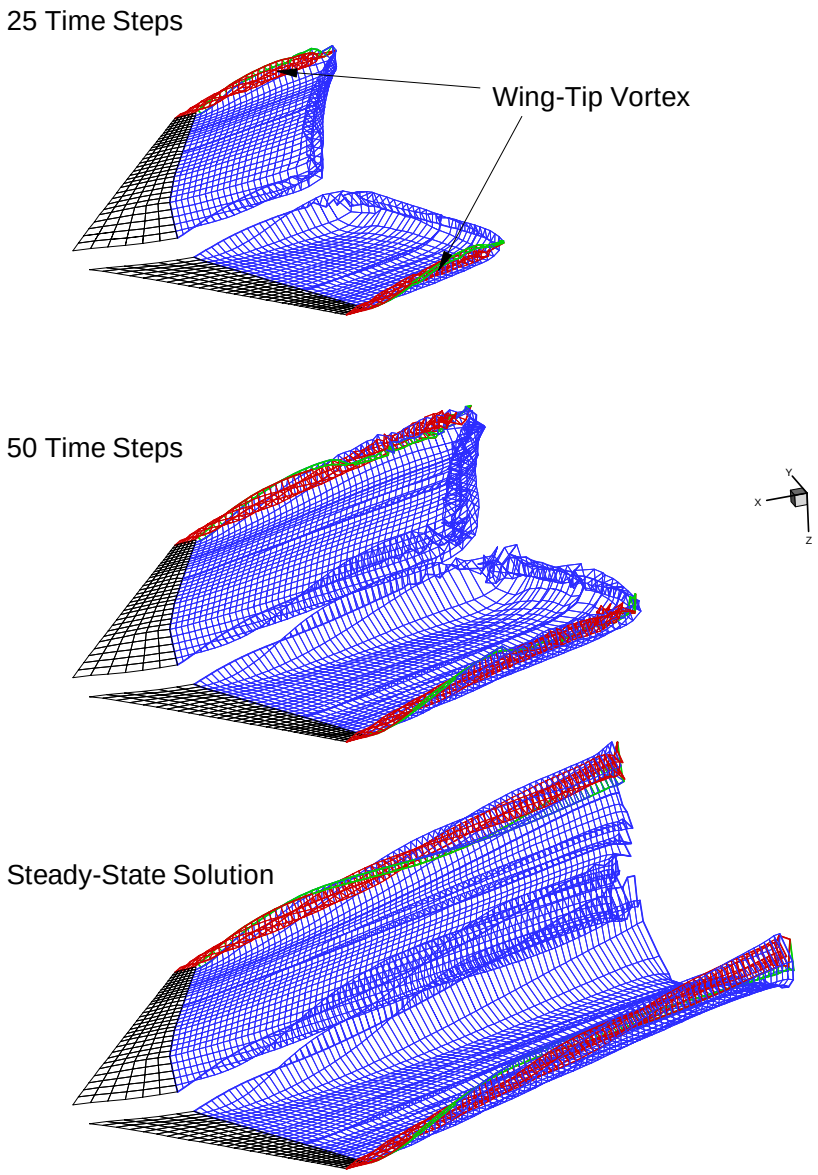

Figure 2-25: The solutions after 25 and 50 time steps, and the steady-state solution.

Figure 2-26: A photograph showing the wing-tip-vortex flowfield.

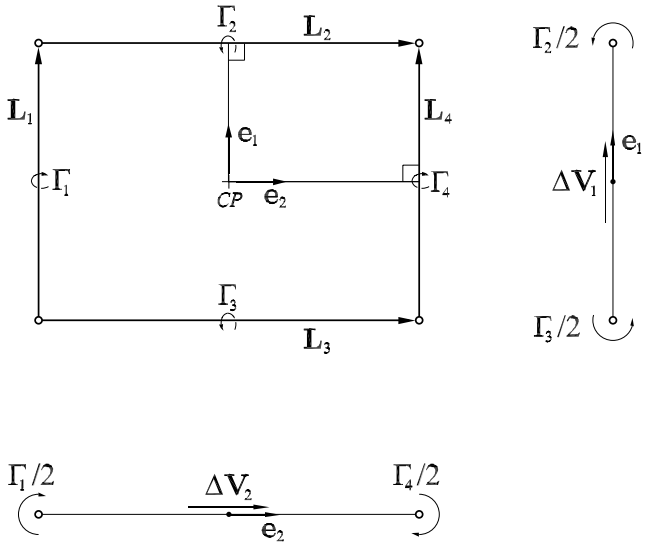

Figure 2-27: A typical rectangular element.

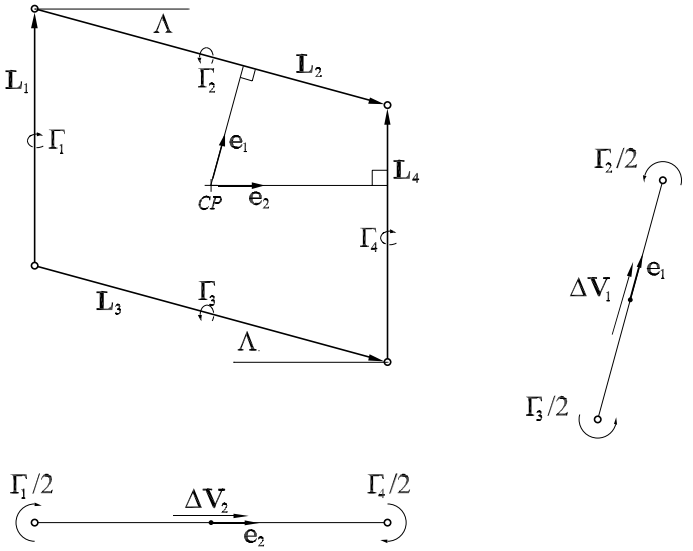

Figure 2-28: A typical parallelogram element.

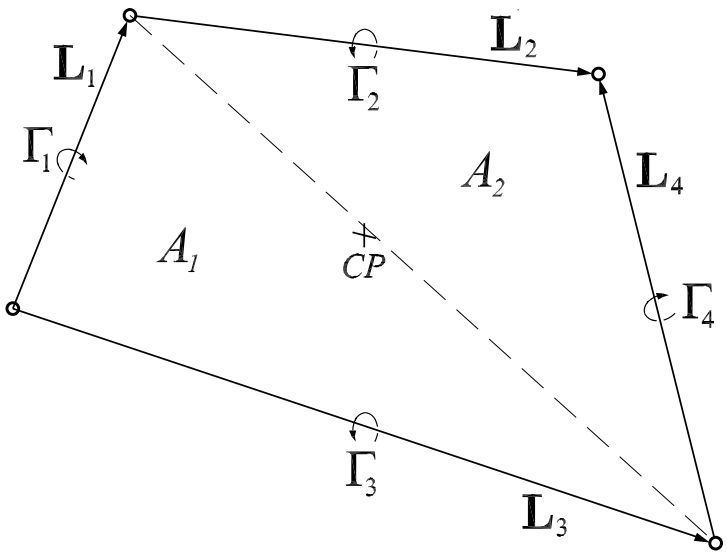

Figure 2-29: A general element.

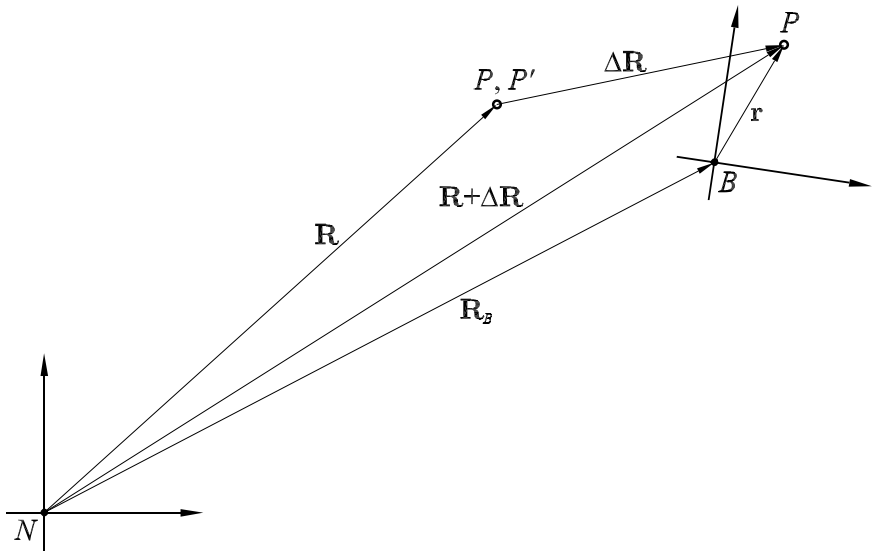

Figure 2-30: The choice of $\mathbf{\Delta R}$.

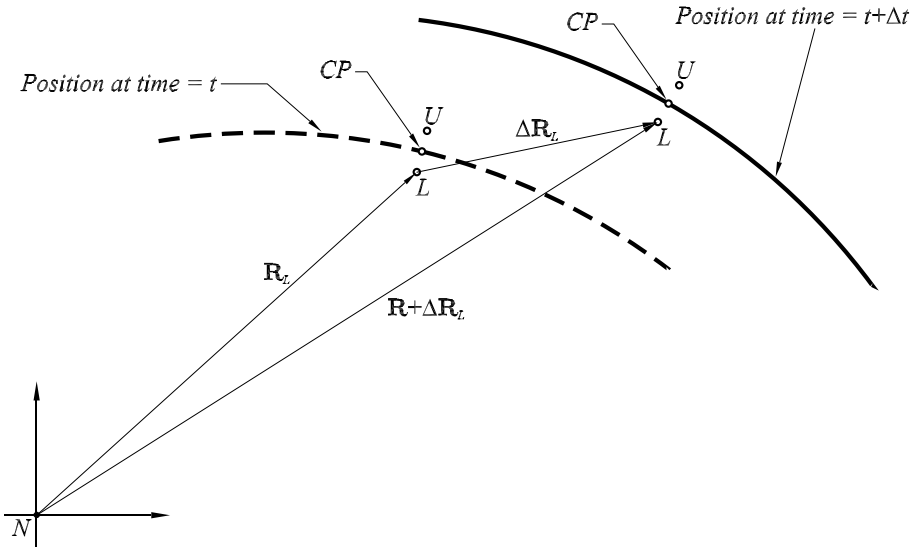

Figure 2-31: The two points used in the evaluation of $\dfrac{\partial \Phi}{\partial t}$.

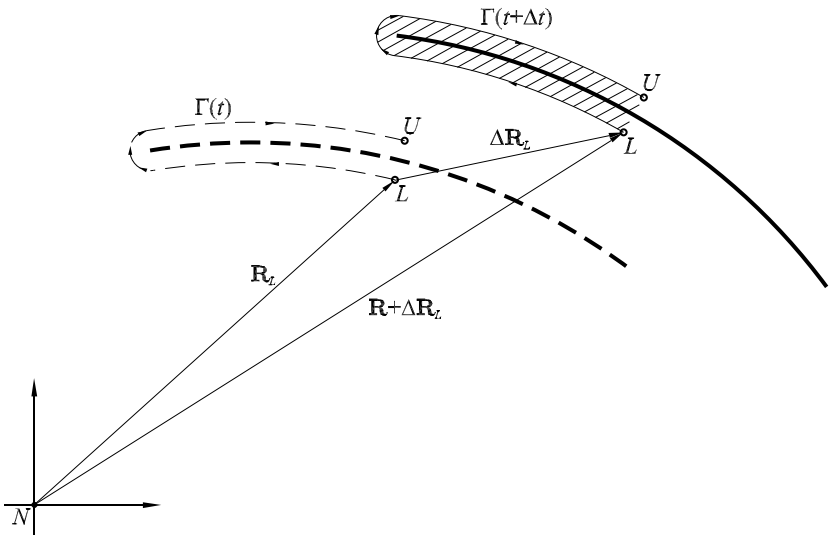

Figure 2-32: The computation of $\Phi(\mathbf{R}_U, t) - \Phi(\mathbf{R}_L, t)$.

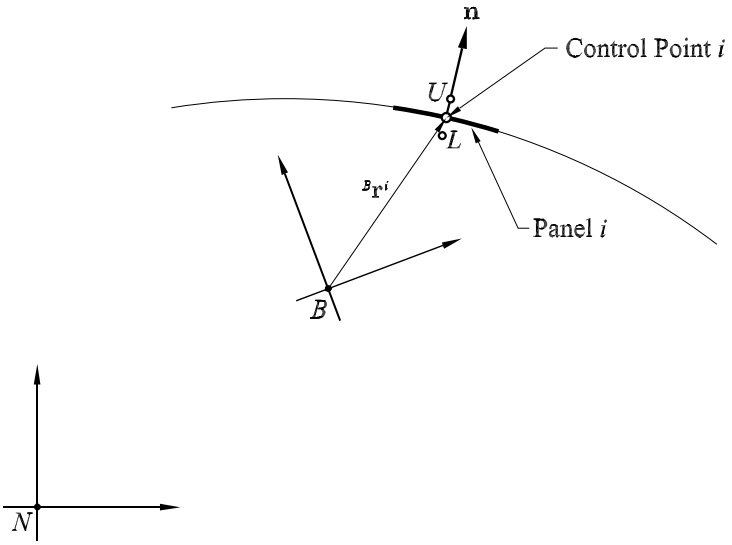

Figure 2-33: The evaluation of $\dfrac{\partial \Phi}{\partial t}(\mathbf{R}_U, t) - \dfrac{\partial \Phi}{\partial t}(\mathbf{R}_U, t)$ at control point i.

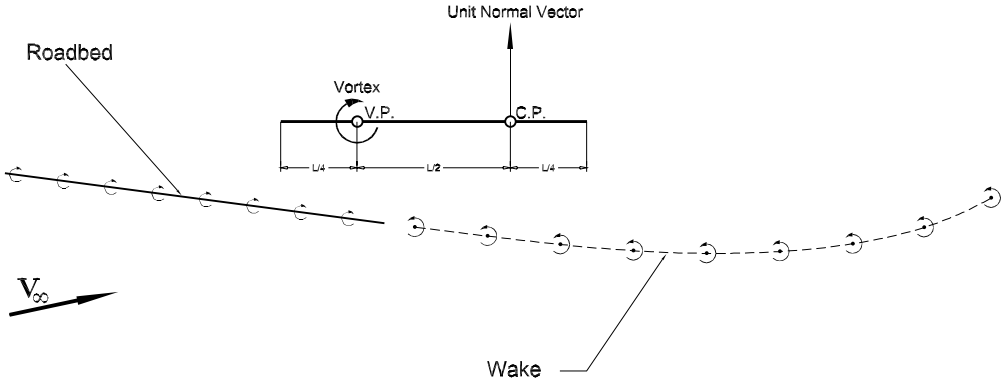

Figure 2-34: Sketch of the aerodynamic model used in Bridge One.

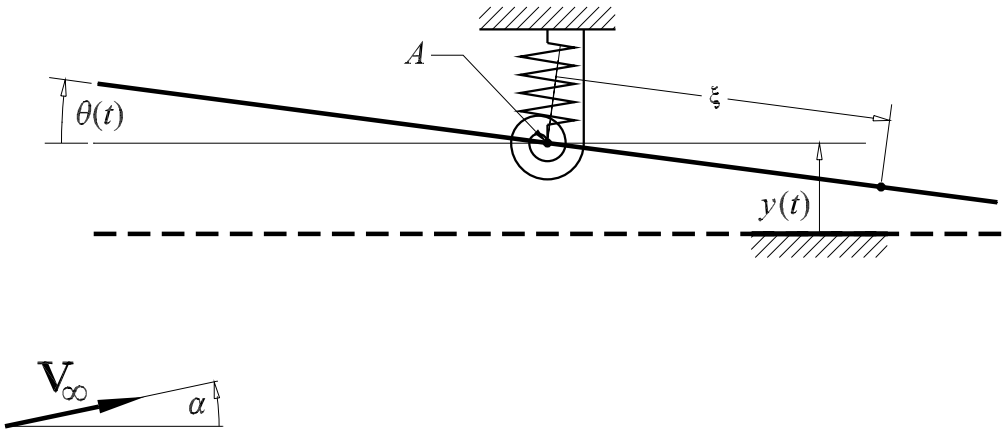

Figure 2-35: The geometry of Bridge One.

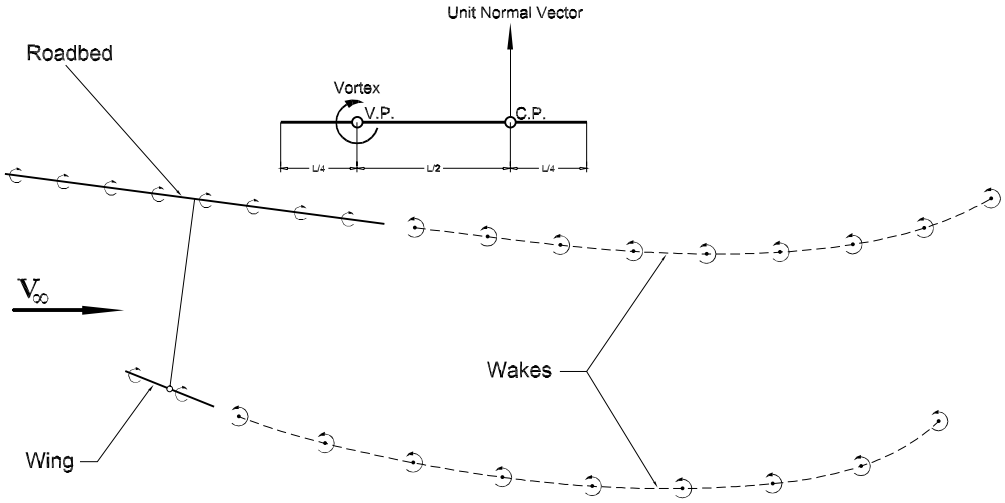

Figure 2-36: Sketch of the aerodynamic model used in Bridge Two.

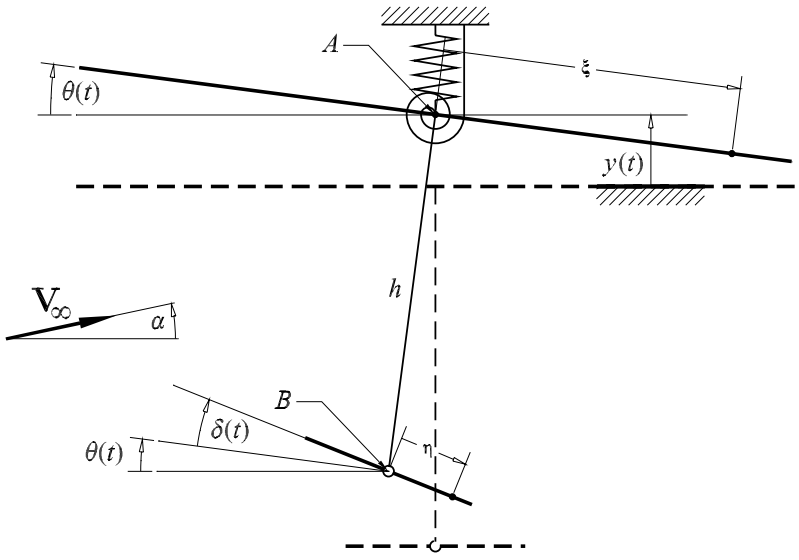

Figure 2-37: The geometry of Bridge Two.

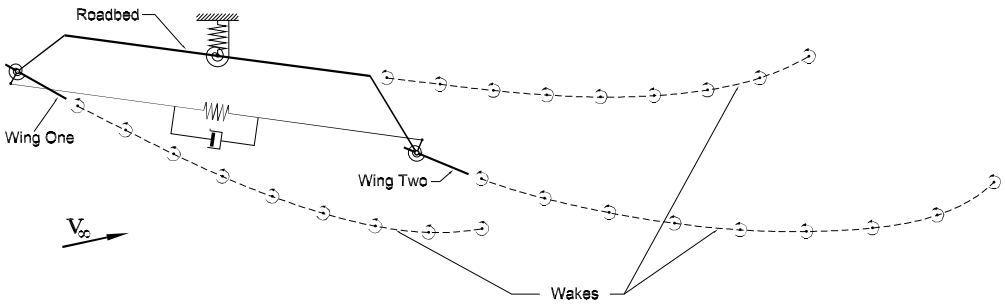

Figure 2-38: Sketch of the aerodynamic model used in Bridge Three.

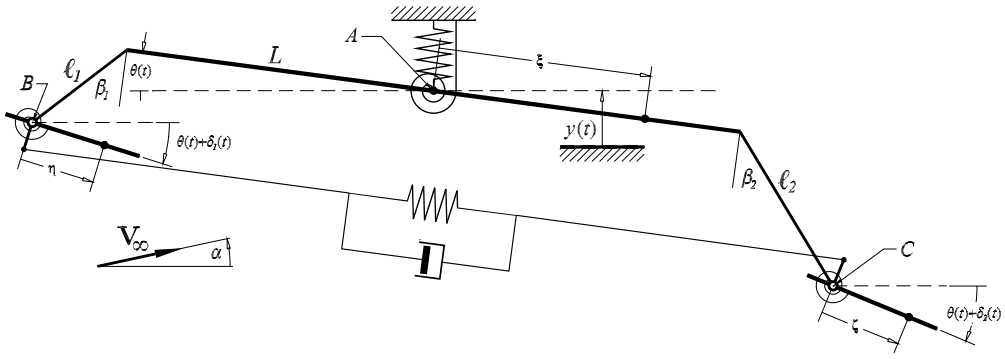

Figure 2-39: The geometry of Bridge Three.